JGR Atmospheres

RESEARCH ARTICLE
10.1029/2018JD029068

Production of Secondary Organic Aerosol During Aging of Biomass Burning Smoke From Fresh Fuels and Its Relationship to VOC Precursors

A. T. Ahern[1,2], E. S. Robinson[1], D. S. Tkacik[1], R. Saleh[3], L. E. Hatch[4,5], K. C. Barsanti[4,5], C. E. Stockwell[6], R. J. Yokelson[6], A. A. Presto[1], A. L. Robinson[1], R. C. Sullivan[1], and N. M. Donahue[1]

[1]Center for Atmospheric Particle Studies, Carnegie Mellon University, Pittsburgh, PA, USA, [2]Now at CIRES, University of Colorado, Boulder, CO, USA, [3]College of Engineering, University of Georgia, Athens, GA, USA, [4]Civil and Environmental Engineering, Portland State University, Portland, OR, USA, [5]Now at Department of Chemical and Environmental Engineering and College of Engineering–Center for Environmental Research and Technology (CE-CERT), University of California, Riverside, CA, USA, [6]Department of Chemistry, University of Montana, Missoula, MT, USA

This article is a companion to Tkacik et al. (2017), https://doi.org/10.1002/2016JD025784.

Key Points:
- We investigated formation of secondary organic aerosol from biomass burning smoke using dual smog chamber experiments
- We used a tracer ion to help quantify secondary aerosol formation, independent of particle wall loss and changing collection efficiency
- Secondary organic aerosol measured agreed within a factor of 2 with that predicted using a scaled, fuel-specific, emission inventory

Supporting Information:
- Supporting Information S1
- Table S1
- Data Set S1

Correspondence to:
N. M. Donahue,
nmd@cmu.edu

Citation:
Ahern, A. T., Robinson, E. S., Tkacik, D. S., Saleh, R., Hatch, L. E., Barsanti, K. C., et al. (2019). Production of secondary organic aerosol during aging of biomass burning smoke from fresh fuels and its relationship to VOC precursors. *Journal of Geophysical Research: Atmospheres*, *124*, 3583–3606. https://doi.org/10.1029/2018JD029068

Received 30 MAY 2018
Accepted 21 JAN 2019
Accepted article online 1 MAR 2019
Published online 28 MAR 2019

Author Contributions:
Conceptualization: R. J. Yokelson, A. L. Robinson, R. C. Sullivan, N. M. Donahue
Formal analysis: A. T. Ahern, E. S. Robinson
Funding acquisition: A. L. Robinson, R. C. Sullivan, N. M. Donahue
Investigation: E. S. Robinson, D. S. Tkacik, R. Saleh, L. E. Hatch, K. C. Barsanti, C. E. Stockwell, A. A. Presto
Methodology: A. T. Ahern, N. M. Donahue
(continued)

Abstract After smoke from burning biomass is emitted into the atmosphere, chemical and physical processes change the composition and amount of organic aerosol present in the aged, diluted plume. During the fourth Fire Lab at Missoula Experiment, we performed smog-chamber experiments to investigate formation of secondary organic aerosol (SOA) and multiphase oxidation of primary organic aerosol (POA). We simulated atmospheric aging of diluted smoke from a variety of biomass fuels while measuring particle composition using high-resolution aerosol mass spectrometry. We quantified SOA formation using a tracer ion for low-volatility POA as a reference standard (akin to a naturally occurring internal standard). These smoke aging experiments revealed variable organic aerosol (OA) enhancements, even for smoke from similar fuels and aging mechanisms. This variable OA enhancement correlated well with measured differences in the amounts of emitted volatile organic compounds (VOCs) that could subsequently be oxidized to form SOA. For some aging experiments, we were able to predict the SOA production to within a factor of 2 using a fuel-specific VOC emission inventory that was scaled by burn-specific toluene measurements. For fires of coniferous fuels that were dominated by needle burning, volatile biogenic compounds were the dominant precursor class. For wiregrass fires, furans were the dominant SOA precursors. We used a POA tracer ion to calculate the amount of mass lost due to gas-phase oxidation and subsequent volatilization of semivolatile POA. Less than 5% of the POA mass was lost via multiphase oxidation-driven evaporation during up to 2 hr of equivalent atmospheric oxidation.

Plain Language Summary We measured aging of biomass-burning smoke at the Missoula Fire Laboratory. The smoke was from various fuels containing green foliage as well as some grasses. We observed significant changes in the mass spectra from the particles, and were also in many cases able to describe formation of additional (secondary) mass to within about a factor of 2 based on measured emissions of volatile organic compounds. However, we show that the amount of secondary mass depends heavily on the type of biomass fuel (green foliated branches vs dried firewood vs grasses, etc).

1. Introduction

Biomass burning is the second largest source of nonmethane volatile organic compounds (VOCs) on Earth (Akagi et al., 2011; Bond et al., 2013; Reid et al., 2005). After emission, these VOCs are diluted by mixing with background air and may subsequently be oxidized. Some compounds that result from the oxidation of these VOCs have sufficiently low volatility to partition into the particle phase; they are known as secondary organic aerosol (SOA; Donahue et al., 2009; Hallquist et al., 2009; Jimenez et al., 2009; Odum et al., 1996). SOA affects important particle characteristics like size, optical properties, and atmospheric lifetimes and contributes significantly to the burden of particulate matter mass. It is thus important to understand and be able to accurately predict SOA formation. Because biomass smoke also contains substantial primary organic aerosol (POA), SOA formation has been measured in part by calculating the enhancement in total organic aerosol (OA) resulting from atmospheric aging (Akagi et al., 2012; Hennigan et al., 2011;

Project administration: R. J. Yokelson
Resources: N. M. Donahue
Supervision: N. M. Donahue
Writing - original draft: A. T. Ahern
Writing – review & editing: D. S. Tkacik, R. Saleh, L. E. Hatch, K. C. Barsanti, C. E. Stockwell, R. J. Yokelson, A. A. Presto, A. L. Robinson, R. C. Sullivan, N. M. Donahue

Yokelson et al., 2009). The OA enhancement is commonly reported in field measurements; it is defined as the ratio of OA mass after aging to the OA mass before aging (the POA) and usually utilizes a functionally inert chemical tracer to account for dilution (Aiken et al., 2010; Bian et al., 2015; Reid et al., 1998; Yokelson et al., 2009).

Cubison et al. (2011) provided an excellent overview of OA enhancements observed in field observations affected by biomass burning. They report an average OA enhancement of 1.19 but also emphasize the range of OA enhancements that have been reported with the standard deviation of 0.18. Early measurements of biomass burning aerosol in Brazil by Reid et al. (1998) showed OA mass enhancements of 1.2–1.4 and speculated that much of the initial growth occurred during the initial few hours. Yokelson et al. (2009) measured the OA mass in a biomass burning smoke plume in the Yucatan, Mexico. After 1.5 hr of aging, and accounting for dilution using carbon monoxide as a conserved tracer, they reported a doubling of OA mass (OA enhancement = 2.0), suggesting significant condensation of SOA. After 2.5 hr of aging in southern Africa, one team reported an OA enhancement of 4 (Vakkari et al., 2014). Decarlo et al. (2010) reported an OA enhancement of ~1.32–1.44 within the first few hours, and up to a day, during the MILAGRO campaign. In contrast, measurements of biomass burning aerosol in West Africa by Capes et al. (2008) reported no enhancement in OA (OA enhancement = 1.) Other field measurements have observed little or no increase in OA mass, although the OA almost invariably became much more oxidized with aging (Akagi et al., 2012; Jolleys et al., 2012). In an effort to identify the cause of the observed variability in SOA production from aged biomass burning emissions, smog chambers have been used to allow sampling of emissions from specific fuels with reproducible oxidation chemistry that simulates atmospheric aging (Bruns et al., 2016; Grieshop, Donahue,& Robinson, 2009; Hennigan et al., 2011; Tiitta et al., 2016).

Unlike more efficient combustion in engines and other engineered devices, *biomass burning* encompasses a vast range of fuels and combustion conditions. Included in this category is dried firewood, as well as standing wood with living foliage, and also dried grass with roots and soil humic matter playing a significant role (Akagi et al., 2011; Andreae & Merlet, 2001). Fires can be intense and flaming, with generally high black carbon emissions, or predominantly smoldering, with generally high OA emissions (Kortelainen et al., 2018; McMeeking et al., 2009; Radke et al., 1991; Yokelson et al., 2003). Given this variability, it is not surprising that observations on SOA formation and other smoke properties are divergent. For example, dried wood not only lost water but also many volatile organic compounds (a dried log is less dense and also less fragrant than a green one). Grass fires and other surface combustion can add soil minerals and inorganic components to the emissions (Ahern et al., 2018; Andreae et al., 2004; Reid et al., 1998). Because of the variability in fuel characteristics and burning conditions, there is an ongoing need for experiments that explore the range of significant fuel and fire types while maintaining a degree of control to enable generalization.

In order to understand SOA production in ambient biomass burning plumes, both the dilution and oxidation processes must be investigated. We thus participated in the collaborative Fourth Fire Lab at Missoula Experiment (FLAME-IV; Hatch et al., 2015; Stockwell et al., 2014, 2015; Tkacik et al., 2017), studying biomass smoke aging from combustion of fresh branches and leaves and grasses through oxidation in dual 7-m^3 smog chambers after dilution of the fresh smoke by approximately a factor of 25. Such dilution reproduces some of the atmospheric dynamics of a smoke plume, including reducing the amount of OA present in the smoke. At lower mass concentrations of OA, more compounds partition significantly into the gas phase from the particle phase, depending on their vapor pressure and activity in the condensed phase (Donahue et al., 2006; Donahue, Epstein, et al., 2011; Pankow, 1994). Some of the POA is semivolatile at ambient conditions (Grieshop, Donahue, & Robinson, 2009; Hennigan et al., 2011; May et al., 2013; Robinson et al., 2007). Furthermore, photochemical processing by hydroxyl radicals is enhanced when semivolatile POA molecules are in the gas phase because they are more accessible than when they reside in the condensed aerosol phase (Donahue et al., 2013; Hennigan et al., 2010, 2011).

Aerosol mass spectrometry provides both quantitative mass measurements and compositional information, albeit with extensive fragmentation of organic compounds. This extensive fragmentation typically requires that POA and SOA be identified based on characteristic ions, with scaling defined by a reference mass spectrum. For example, both Sage et al. (2008) and Grieshop, Donahue, and Robinson (2009) used the mass spectrum of POA prior to aging to calculate SOA mass produced in smog-chamber aging experiments. However, this method of calculating SOA mass assumes that POA is only lost via particle-to-wall deposition

(neglecting POA vaporization or oxidation) and also that the contribution of SOA to the chosen POA marker ions is negligible. For example, the marker used by Sage et al. (2008) was the signal at m/z 57 at unit mass resolution, which also features prominently in SOA mass spectra (Ulbrich et al., 2009). Thus, the calculated SOA mass may be underestimated if the POA mass spectrum is scaled by an ion also produced from the fragmentation of SOA components. Alternatively, the calculated SOA mass may be overestimated if the POA mass spectrum is scaled by an ion produced by a semivolatile or reactive/nonconserved POA compound. Hennigan et al. (2011) calculated an upper estimate of POA that may be oxidized, using levoglucosan—a product of cellulose pyrolysis—as a tracer for POA. They found that for their smog-chamber experiments using biomass burning emissions from highly diluted "chamber burns" of various fuels including branches and leaves, only 17% of the OA mass after aging was POA. However, levoglucosan is semivolatile (May et al., 2012). For this work, we selected a different tracer to avoid both potential problems: nonconservative/nonunique POA and SOA markers and also dilution/evaporation of selected markers. We present evidence that in these experiments, the ion $C_7H_{11}^+$ (m/z 95.086) is produced mainly from low-volatility POA compounds, with minimal influence from compounds present in SOA. It is therefore suitable for use as a POA tracer ion to calculate both the POA mass lost through evaporation/oxidation and the new SOA mass condensed.

Having measured the amount of SOA formed in FLAME-IV experiments, we compared the measured SOA with the amount predicted based on the extensive gas-phase characterization of VOCs understood to contribute to SOA formation through oxidation and condensation. Recent studies have investigated the emissions of dried logwood fires in residential woodstoves, which by design produce more consistent combustion conditions than in open burning. Those investigators were able to predict the amount of SOA measured in their smog-chamber experiments using relatively few traditional VOC SOA precursors (e.g., toluene, benzene, and α-pinene; Bruns et al., 2016; Tiitta et al., 2016). However, the biomass burned in our experiments typically contained foliage in addition to logwood. It was also relatively fresh as opposed to dried firewood and was burned in an open, scattered arrangement rather than in a residential woodstove. Stockwell et al. (2014, 2015, 2016) showed that the VOC mass emissions from simple cookstoves were much lower than those from uncontained fires. Furthermore, Hatch et al. (2015) showed using two-dimensional gas chromatography (GC × GC-TOFMS) that the composition of the VOCs emitted in FLAME-IV varied significantly depending on the fuel burned.

All of these factors motivated our design and analysis methods for these smog-chamber aging experiments. In this work, we sought to measure SOA formation from fuels and burn conditions representative of open biomass burning, rather than more efficient combustion conditions, for example, kiln-dried hardwood or pellets in stoves (Bruns et al., 2016; Czech et al., 2017; Tiitta et al., 2016). We analyzed the varying composition of the OA as a result of aging, using a POA tracer ion to more precisely measure the counterbalancing effects of POA evaporation and SOA condensation on total OA mass. Using the comprehensive gas-phase characterization of emissions available for the fuels burned during FLAME-IV, we were able to estimate how much of each of the 674 identified VOCs were present in the beginning of a smog-chamber experiments. For some of these VOCs, there are known reaction rate constants with OH and SOA yields. For others, reasonable assumptions must be made based on structural and functional similarities with VOCs for whom these properties are known, following the suggestions described in Hatch et al. (2015). For simplicity, we assume that the SOA produced is nonvolatile. Despite this simplification and necessary but unconstrained assumptions about SOA production from VOCs without published SOA yields or OH reaction rate constants, we can predict SOA formation within a factor of 2 for these smog-chamber experiments using biomass burning aerosol.

2. Materials and Methods

2.1. Experimental Methods

We performed smog-chamber experiments during FLAME-IV using dual smog chambers that enabled paired experiments on the same smoke aerosol from the same biomass fuel burn. Tkacik et al. (2017) provide a detailed description of the Dual Chamber Experiment method, and Stockwell et al. (2014) provide a comprehensive description of the fuels burned and the combustion conditions used. Thus, we provide only a brief description here.

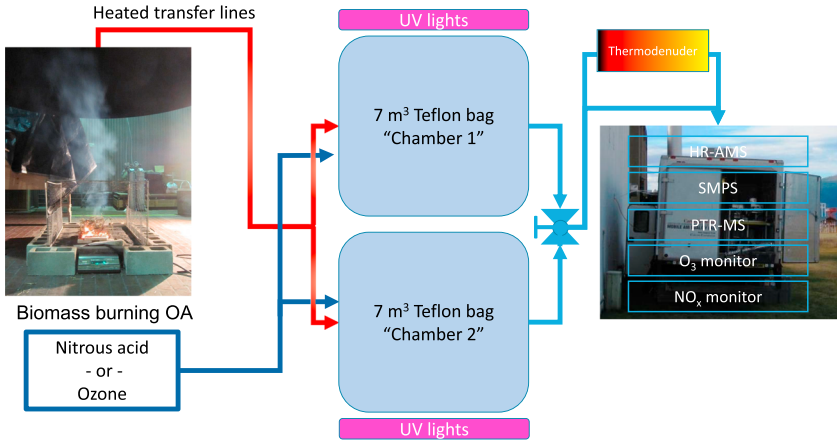

Figure 1. The experimental setup at the Fire Laboratory in Missoula Experiments, FLAME-IV. Biomass was burned in the Missoula Fire Lab facility and transferred via heated transfer lines to two identical smog chambers. The smog chambers could independently simulate three types of aging: UV photolysis, UV photolysis with nitrous acid (HONO), or dark ozonolysis. Instrumentation in the CMU mobile lab characterized the emissions during the experiments using an automated valve system to switch between the two chambers.

We burned a variety of biomass fuels and injected the resulting smoke into a pair of identical 7-m^3 Teflon environmental chambers, located inside the 3,000-m^3 combustion chamber at the Missoula Fire Sciences Lab. Globally relevant fuels discussed in this paper include agricultural residue, grasses, tree boughs, and peat collected from North America, Africa, and Asia (Stockwell et al., 2014). Before each burn, we loosely scattered or propped up the biomass fuel on the ignition platform, simulating open burning conditions. We then ignited the fuel using a resistive heating element or a propane torch.

We show a schematic of the experimental setup in Figure 1. Prior to each experiment, we purged the dual smog chambers for 12 hr with dry, particle-free, and VOC-scrubbed air. We used UV radiation from black lights (GE model 10526) positioned underneath the chambers to assist in cleaning the chambers. At the beginning of an experiment, we filled the two dark chambers with smoke pulled through heated (40 °C), passivated, and smoke-conditioned transfer lines by four Dekati eductor diluters (Tkacik et al., 2017). For some experiments, we sampled smoke from the well-mixed plume in the Fire Lab smoke stack. These experiments are identified as *stack burns*, and smog chamber filling took place while most of the fuel was consumed, including the flaming phase and most of the smoldering phase. We stopped filling the chambers when the fire visually appeared to be emitting very little smoke. Alternatively, the stack was sealed and the ignited biomass was allowed to burn completely, filling the entire Fire Lab combustion chamber. These experiments are called *room burns*, and for these cases we sampled the smoke from 2 m off the ground, reducing the transfer line from 15 (for stack burns) to 3 m (for room burns). While the stack burns were designed to collect most of the smoldering phase emissions, we sealed the chambers when there was visually little smoke being emitted from the fire. This allowed a faster commencement of the experiment, reducing the opportunity for particles or gases to come into contact with smog chamber walls prior to oxidation. In contrast, room burns were allowed to become well mixed in the Fire Lab, and therefore, all of the smoldering emissions were included in the sample pulled into the smog chambers.

After we sealed the chambers, we allowed the contents to become well mixed and then characterized each chamber in sequence. We sampled the aerosol from the dual chambers through passivated 3/8″ O.D. stainless-steel tubing that was actively maintained at 40 °C with a suite of instruments located outside the Fire Lab in the CMU mobile lab. Two automated three-way ball valves allowed for the gas and particle instrumentation to switch between sampling from either one of the two chambers.

After initial characterization, 15 to 45 min after smoke injection, we perturbed the contents of a chamber in one of three ways: (1) using UV lights to initiate photochemistry and generate hydroxyl radicals (OH) from existing precursors, (2) injecting nitrous acid (HONO) in addition to the UV lights to augment the OH concentration, or (3) injecting an excess of ozone (>500 ppbv). We generated and injected HONO from a

solution of H_2SO_4 and $NaNO_2$ via the method described in Ng et al. (2007). We generated ozone separately via corona discharge in the presence of pure oxygen. We also conducted control experiments periodically with no perturbation to one or both chambers. In these cases, suspended particle concentrations decreased due to loss to the walls and measured VOC concentrations remained constant. We list each experiment in Table 1, indexed according to the burn identification convention in Stockwell et al. (2014). The additional hyphenated number (1 or 2) is used to separate the two different smog chambers filled with smoke diluted from the same fuel. Table 1 also contains details regarding initial OA concentrations and composition.

2.2. Characterizing the Particulate Phase

We quantified black carbon (BC) using a Single-Particle Soot Photometer (SP2, Droplet Measurement Technologies) and a seven-wavelength aethalometer (McGee Scientific model AE-31; Saleh et al., 2014). Since black carbon is inert and nonvolatile with no sources after smoke injection, it has been used in past chamber experiments to measure the rate at which aerosol particles were lost to the walls (Hennigan et al., 2011; Tkacik et al., 2017). In this work we present BC mass measurements as a motivator for exploring the use of our POA tracer ion method; we present a comparison of the two methods in the Supporting Information, Figure S1. We discuss challenges associated with using BC mass as a metric for particle wall loss in section 2.3.

We measured total particle number and mobility diameter size distributions using a scanning mobility particle sizer (SMPS, Model 3081: 3080 DMA and 3021 butanol CPC; TSI, Inc.), characterizing particles from 10.7 to 478 nm in mobility diameter. We measured speciated nonrefractory aerosol mass and chemical composition using an Aerodyne high-resolution aerosol mass spectrometer (AMS). The AMS measures particulate matter that has a vacuum aerodynamic diameter between 70 and 700 nm and that vaporizes upon contact with a 600 °C heater in vacuum (Decarlo et al., 2006; Jayne et al., 2000). A thermodenuder with an automated by-pass switching valve was placed in line with the AMS. We ramped the thermodenuder as high as 250 °C to evaluate the volatility the aerosol (Huffman et al., 2008). We performed high-resolution peak fitting and attribution of the AMS signal using PIKA 1.12 and calculated the oxygen-to-carbon elemental ratio (O:C) using the method described by Canagaratna et al. (2015). For quantitative mass measurements of organic aerosol with the AMS, the collection efficiency with respect to particle bounce is very important. To address the possibility of changing collection efficiencies as a result of changing OA composition during aging, we use a POA tracer ion as a naturally occurring internal standard, specifically $C_7H_{11}^+$. We used peak fitting of high-resolution AMS data at *m/z* 95 to quantify $C_7H_{11}^+$, *m/z* 95.086 (see Supporting Information Figure S2). By using a POA tracer ion, we can relate the OA mass of aged smoke that has an unknown collection efficiency, with the OA mass of fresh smoke that likely has a collection efficiency equal to 1. For fresh biomass burning aerosol, we used a collection efficiency of 1.0, consistent with past observations of primary and aged emissions from biomass burning (Hennigan et al., 2011; Heringa et al., 2011).

2.3. Characterizing Particle Wall Loss

Calculating OA enhancements in smog-chamber experiments requires quantification of the particles and vapors lost to the Teflon walls. When possible, it is common to calculate the particle wall loss using BC as a POA tracer and the total aerosol mass concentration from measurements made by either an SMPS or AMS (Grieshop, Donahue, & Robinson, 2009; Hennigan et al., 2011; Heringa et al., 2011; Tiitta et al., 2016). However, at high concentrations (greater than 12,500 particles cm^{-3}) the SP2 may become saturated, causing it to undercount the number of BC-containing particles. Likewise, SOA production can bias aethalometer measurements due to increased absorption due to lensing and/or brown carbon (Heringa et al., 2011; Saleh, Donahue & Robinson, 2013). Thus, although BC in theory makes an excellent tracer species for particle wall loss, the difficulty associated with its precise measurement creates some challenges in practice. Furthermore, during the aging process physicochemical properties of the particles are changing, and this may lead to bias in calculated OA enhancements. For example, particle density may change due to the condensation of SOA, or the particle collection efficiency of the AMS may change, due to changes in particle composition, physical state, and viscosity (Donahue et al., 2013; Robinson et al., 2017). Primary biomass burning emissions are typically quantified assuming no particle bounce (collection efficiency = 1.0), but secondary organic aerosol can have a collection efficiency of 0.5 or lower (Docherty et al., 2013; Hennigan et al., 2011; Robinson et al., 2017). While a changing collection efficiency can affect the total signal from an ion in the mass spectrum, it will not change its *fractional* contribution to the total ion signal for an

Table 1
Experimental Details for Each Pair of Smog Chamber Experiments

Burn number-chamber	Date	Fuel	Perturbation type	Organic aerosol[a] ($\mu g/m^3$)	O:C	$NO + NO_2$ (ppb)	Initial toluene (ppb)	OA enhancement after 1.5 hr	SOA mass produced $\omega = 1$	Ratio of SOA predicted versus measured
84-1	10/21/2012	Ponderosa pine	HONO + UV	65	0.21	n/a	2.5	1.40	25.8	
84-2	10/21/2012	Ponderosa pine	UV only	57	0.21	n/a	3.0	1.48	27.9	
115-1	10/23/2012	Ocote	UV only	1	0.16	1	0.6	1.37	0.4	
115-2	10/23/2012	Ocote	Ozone	1	0.13	0	0.5	3.09	0.3	
126-1	10/24/2012	Black spruce	HONO + UV	5	0.16	100	0.6	1.22	1.0	
126-2	10/24/2012	Black spruce	UV only	4	0.17	11	0.7	1.49	2.0	
127-1	10/25/2012	Ponderosa pine	Dark	60	0.16	11	1.7	0.97	−3.3	
127-2	10/25/2012	Ponderosa pine	UV only	56	0.17	13	2.0	1.18	18.4	
131-1	10/28/2012	Black spruce	Dark	16	0.20	3	0.7	0.93	−1.3	
131-2	10/28/2012	Black spruce	UV only	11	0.20	2	0.6	1.04	1.1	0.66
134-1	10/29/2012	Black spruce	Dark	105	0.22	32		0.98	−2.1	
134-2	10/29/2012	Black spruce	Ozone	64	0.22	24		1.45	33.0	
137-1	10/30/2012	Black spruce	Dark	67	0.23	29		0.97	−3.1	
137-2	10/30/2012	Black spruce	UV only	47	0.23	26		1.15	10.5	
140-1	10/31/2012	Ponderosa pine	HONO + UV	184	0.21	643		1.06	26.5	
140-2	10/31/2012	Ponderosa pine	UV only	121	0.22	12		1.04	22.0	
142-1	11/1/2012	Ponderosa pine	Dark	39	0.23	18	1.2	1.00	0.1	
142-2	11/1/2012	Ponderosa pine	Ozone	36	0.23	19	1.2	1.16	12.8	2.65
144-1	11/3/2012	Ponderosa pine	UV only	117	0.22	10	1.3	1.02	8.7	0.15
144-2	11/3/2012	Ponderosa pine	Ozone	137	0.21	12	1.8	1.29	48.0	0.59
146-1	11/4/2012	Organic hay	Dark	130	0.14	19	3.8	0.97	−3.6	
146-2	11/4/2012	Organic hay	UV only	145	0.14	23	4.4	1.17	52.5	
148-1	11/5/2012	Giant cutgrass	Dark	7	0.26	20	0.9	0.97	−0.5	
148-2	11/5/2012	Giant cutgrass	UV only	9	0.24	24	1.0	1.04	0.7	2.69
151-1	11/6/2012	Wiregrass	UV only	15	0.43	21	0.7	1.01	0.4	
151-2	11/6/2012	Wiregrass	Dark	15	0.41	23	0.7	1.10	2.0	0.68
153-1	11/7/2012	Rice straw	Dark	19	0.22	46	1.8	1.01	0.1	
153-2	11/7/2012	Rice straw	UV only	16	0.23	45	1.8	1.10	3.7	2.76
154-1	11/8/2012	Peat	Ozone	28	0.10	2	0.9	1.06	2.6	4.08
154-2	11/8/2012	Peat	UV only	27	0.10	2	0.8	1.05	1.5	0.09
155-1	11/10/2012	Black spruce	HONO + UV	84	0.25	1386	2.1	1.10	13.0	2.11
155-2	11/10/2012	Black spruce	UV only	91	0.24	10	2.0	1.08	14.0	1.90
156-1	11/11/2012	Black spruce	Ozone	66	0.26	50	2.0	1.40	24.0	1.00
156-2	11/11/2012	Black spruce	Ozone	67	0.26	12	1.8	1.20	20.1	1.74
157-1	11/12/2012	Black spruce	UV only	85	0.27	13	2.6	1.09	16.1	2.82
157-2	11/12/2012	Black spruce	Ozone	76	0.27	13	2.5	1.36	29.4	1.18

[a]Organic aerosol concentration after injection, but before perturbation at beginning of experiment.

internally mixed aerosol. Thus, if one uses the relative contribution of ions in the OA mass spectra, changes in particle density and collection efficiency are internally corrected. While useful, this method is dependent on the premise that the aerosol population is homogenous. Given that the aerosol in a given chamber experiment is generated from a single fire, this is likely a reasonable assumption. The implications of this assumption are discussed in further detail in section 3.3.

In this work, we identify a tracer ion generated from low-volatility molecules that (a) are readily detected in POA and (b) unlikely to have a significant contribution from SOA. We then use the changing relative contribution of this ion signal to the total OA ion signal to calculate both the SOA mass condensed and POA mass evaporated during the chamber experiment. Additional wall-loss corrections are required to account for particle and vapor deposition, but our new method for calculating changes in OA composition using the POA tracer self corrects for any changes in both AMS collection efficiency and particle density. It also reduces the dependence on the potentially inaccurate BC mass measurements.

2.4. Characterizing the Gas Phase

We used a proton transfer reaction mass spectrometer (PTR-MS) to measure in real time the concentrations of selected VOCs. The PTR-MS (Ionicon, GmbH.) measures organic ions formed from charge transfer

between $H_3O^+ \cdot (H_2O)_n$ ($n = 0, 1, 2, ...$) produced in an isolated source and the VOCs in the sampled gas. Each VOC has a specific charge-transfer efficiency that we calibrated weekly with a premixed standard (Scott-Marrin, Inc., Riverside, California) of known concentrations including toluene and acetone, which we discuss below. We operated the quadrupole mass spectrometer of the PTR-MS in selected-ion mode, analyzing with unit mass resolution preselected VOCs listed in the Supporting Information, Table S1. The 1-Hz sampling frequency of the PTR-MS is useful for estimating OH exposure in the chamber, but the PTR-MS cannot differentiate between isomers, such as the many monoterpene isomers that have different chemical structures but the same chemical formula and thus same molecular weight. Analysis of fresh smoke from these experiments by GC × GC-TOFMS showed that no significant toluene isomers were detected in the fresh smoke (Hatch et al., 2015); thus, the PTR-MS can accurately report toluene concentrations. We used the following first-order reaction equation for toluene to calculate the average OH concentration in each chamber:

$$\frac{C_t}{C_0} = e^{-kt[\mathrm{OH}]} \quad (1)$$

where C_0 and C_t are concentrations of toluene measured at the beginning and end of a chamber aging experiment, respectively. We used a rate constant of $k = 5.63 \times 10^{-12}$ $cm^3 \cdot molecule^{-1} \cdot s^{-1}$ (Atkinson & Arey, 2003). When we injected HONO into the smog chambers, the OH concentration was usually about 2×10^6 molecules cm^{-3} versus about 1×10^6 molecules cm^{-3} for UV lights only experiments. For dark ozonolysis experiments, toluene decay calculations indicated that ~2×10^5 OH molecules cm^{-3} were generated by secondary processes (presumably ozonolysis of alkenes).

To provide a more detailed analysis of VOCs, we collected vapor samples onto adsorption-thermal desorption cartridges for offline analysis via GC × GC-TOFMS. The GC × GC-TOFMS analysis has been described in Hatch et al. (2015); briefly, two GC columns are used to separate the gas samples first by volatility and then by polarity. Besides quantitatively measuring 674 compounds, Hatch et al. also put forth a simple framework by which to estimate SOA production from the measured VOC precursors. We will use the same parameters to predict the amount of VOC reacted and subsequent SOA mass formed. Reaction rate constants and assumed SOA yields are listed in the Supporting Information, Table S2.

We measured other gas-phase species including NO_x (= NO + NO_2) via chemiluminescence (Teledyne, model 200EU), carbon dioxide using nondispersive infrared photometry (Licor Biosciences, model LI-820), and ozone by photometry (API, model 400A).

3. Results and Discussion

3.1. Mass Spectra of Organic Aerosol

In Figure 2a we show the high-resolution mass spectrum for the OA component from black-spruce smoke after it was diluted into one of the smog chambers and prior to any aging. The ions are grouped into chemical families according to their oxygen content: C_xH_y (green) has no oxygen, C_xH_yO (purple) has one oxygen atom, and $C_xH_yO_{>1}$ (pink) has more than one oxygen atom (in this case usually two). The abundance of signal from C_xH_y is typical of fresh combustion emissions that have a low oxidation state. The presence of $C_xH_yO_2$ (especially $C_2H_4O_2$ and $C_3H_5O_2$) is consistent with past observations of primary biomass burning OA (Cubison et al., 2011; Hennigan et al., 2011; Ortega et al., 2013); these are fragments from carbohydrates, which are major particulate-phase products of biomass combustion.

We did not attempt to resolve nitrogen containing ions because they cannot be reliably resolved at the V-mode resolution of the HR-TOF-AMS of ~2100 at *m/z* 200. Also, the nitrate group from organic nitrates typically fragments in the vaporizer, producing a characteristically high ratio of NO^+ to NO_2^+ ion signal (*m/z* 30:46) compared to ammonium nitrate (Farmer et al., 2010). Our instrument has a typical NO^+:NO_2^+ of ~0.3 for ammonium nitrate. We measured NO^+ to NO_2^+ ion ratio values for diluted POA ranging from 3.6 to 12.6, suggesting significant organic nitrate content in the fresh, diluted smoke (Farmer et al., 2010; Mohr et al., 2012; Schurman et al., 2015). The measured NO^+:NO_2^+ decreased with time for all chamber experiments, suggesting that pyrogenic ammonia was neutralized by HNO_3 to form NH_4NO_3, thus reducing the relative contribution from organic nitrates to the NO^+ and NO_2^+ ion fragments.

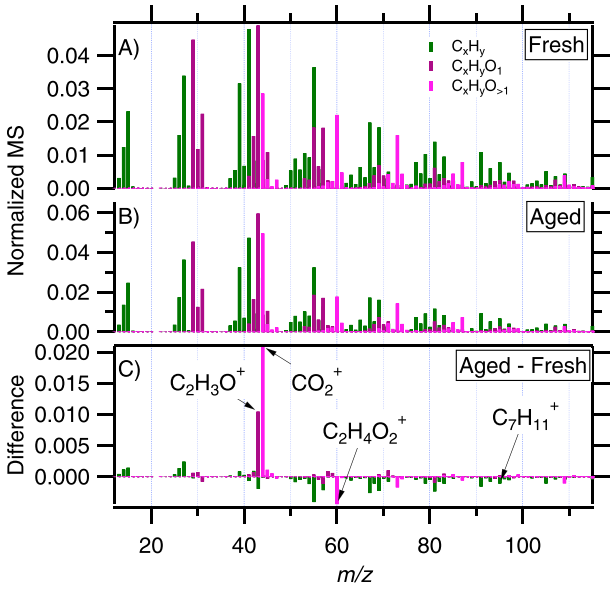

Figure 2. The normalized high-resolution mass spectra of organic aerosol from burning black spruce before (a) and after (b) aging by UV light. Panel (c) shows the difference between the normalized spectra in (a) and (b). Positive values indicate that an ion signal increased following aging, potentially due to the formation of secondary organic aerosol. Negative values may have three different explanations: evaporation of OA, oxidation of OA into VOCs or SOA, or decreased relative contribution due to condensation of SOA.

Figure 2b shows a mass spectrum for the OA from the same black-spruce smoke experiment, after aging via UV light and OH oxidation (no HONO added). To illustrate the differences between the two spectra, and to correct for particle wall loss, we show the difference of the two spectra, each normalized to their total ion signal, in Figure 2c. As this is the difference of normalized spectra, shown in equation (2), positive signals indicate fragment ions that are more abundant in the aged spectrum, and negative signals indicate ions that are more abundant in the fresh spectrum. In equations (2) and (3), MS represents an organic mass spectrum as an array.

$$\mathrm{MS}_{2c} = \frac{MS_{aged}}{\sum MS_{aged}} - \frac{MS_{fresh}}{\sum MS_{fresh}} \quad (2)$$

Ions with a positive value in Figure 2c are therefore SOA products produced during aging. For example, CO_2^+ (*m/z* 44) and $C_2H_3O^+$ (*m/z* 43), which contribute the bulk of the signal here, are strongly associated with SOA (Ng et al., 2010). Ions with negative signals in Figure 2c are predominantly POA, whose relative abundance is lessened by the SOA produced during aging. However, some ions are present in both SOA and POA, which complicates the interpretation of Figure 2c. For example, previous studies have shown that SOA can contribute to signal at *m/z* 55 (mostly $C_4H_7^+$), and thus, although most of the signal at *m/z* 55 is from POA, the reduction may be less than one would expect after aging because of counterbalancing condensation of SOA (Chhabra et al., 2010; Hildebrandt et al., 2009). Besides the condensation of SOA, evaporation or oxidation of POA can also result in a negative difference signal. Normalizing mass spectra by their total signal is a simple method of accounting for changes in total particle signal, but it may underrepresent composition changes from of SOA condensation and POA evaporation.

The family $C_{x>1}H_yO_2$ has several large negative signals, all $C_xH_yO_2$ except for CO_2^+, in Figure 2c, indicating that they correspond to compounds present in the POA. This family includes the ion at *m/z* 60, $C_2H_4O_2^+$, the dominant ion resulting from the fragmentation of levoglucosan in the AMS (Cubison et al., 2011; Hennigan et al., 2010). Levoglucosan is a common biomass burning marker compound arising from the pyrolysis of organic polymers like cellulose (Simoneit et al., 1999). However, Hennigan et al. (2010, 2011) showed that levoglucosan is semivolatile and reacts with OH in the gas phase at a nonnegligible rate. Additionally, although *m/z* 60 has been shown to correlate with levoglucosan, a comparison between AMS data and filter analysis shows that levoglucosan accounts for less than 10% of the total signal at *m/z* 60 (Aiken et al., 2009; Lee et al., 2010; Sullivan et al., 2008); the remainder may come from other cellulose-pyrolysis products and other OA components. Cellulose pyrolysis may also generate a variety of products contributing to other highly oxygenated ions observed in the POA, namely, $C_3H_5O_2^+$ (*m/z* 73) and $C_4H_7O_2^+$ (*m/z* 87). To our knowledge, the effect of atmospheric aging on other ions derived from cellulose pyrolysis components during AMS analysis in the family of $C_{x>1}H_yO_2$ has not yet been investigated. Thus, if one assumes that *m/z* 60 is a conserved POA tracer ion, it will prove difficult to quantify the contribution of POA given that it will decay due to both oxidation and dilution-driven evaporation. Furthermore, the initial signal level of *m/z* 60 in OA depends on the fuel and/or combustion conditions (Lee et al., 2010) and can be produced as part of SOA formation (Fortenberry et al., 2018).

In addition to the oxygenated compounds arising from cellulose pyrolysis, biomass burning POA is also typically rich in chemically reduced fragments, such as *m/z* 55 ($C_4H_7^+$) and *m/z* 57 ($C_4H_9^+$; Ulbrich et al., 2009), consistent with past investigations of emissions from fossil fuel combustion. Another POA ion of interest is $C_7H_{11}^+$ at *m/z* 95.086. Due to the large size of the fragment ion, it is less likely to have significant interference from SOA, as this could only come from secondary molecules with a long (C_7 or longer) aliphatic component. Empirically, a general trend observed in AMS measurements is the loss of larger organic ions as the oxidation state of the OA increases (Canagaratna et al., 2015). This is consistent with larger molecules

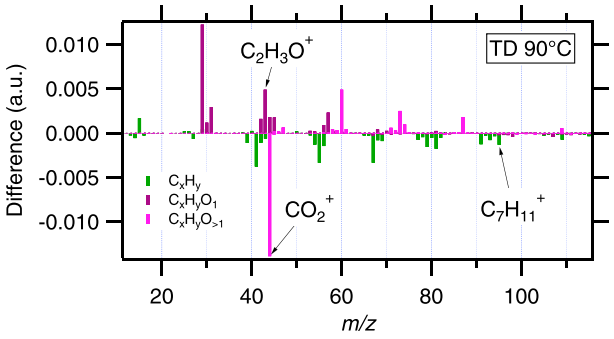

Figure 3. The difference between the normalized mass spectra from thermally denuded and bypass OA is shown for fresh biomass burning aerosol. Positive signals indicate ions associated with more volatile compounds in the OA that were evaporated in the thermodenuder, whereas negative signals indicate ions associated with less volatile compounds that did not evaporate.

becoming oxidized at secondary or tertiary carbons causing fragmentation into smaller, more stable oxygenated fragments upon electron ionization. A primary carbon is unlikely to become oxidized and subsequently ionization to generate a large molecular ion like $C_7H_{11}^+$. If a molecule was sufficiently large that oxidation yielded a $C_7H_{11}^+$ fragment, then it will likely have already have been in the particle phase as POA.

Figure 3 shows a difference spectrum, bypass minus thermodenuded at 90 °C, of the fresh aerosol. Before we take the difference, we normalize these mass spectra by the sum of their total OA ion signal (equation (2)). We normalize the spectra by their total ion signal because the themodenuder will cause a decrease in total ion signal by two processes: evaporation of material from individual particles and loss of whole particles due to thermophoresis, which is independent of volatility. After normalizing the spectra by the total ion signal, the positive values represent fragment ions from molecules that are relatively more abundant in the undenuded spectra and thus more volatile. The negative values represent ions from molecules relatively more abundant in the denuded spectra and therefore less volatile. The signal at CO_2^+ (m/z 44) comes largely from low-volatility oxidized organic compounds, sometimes called LVOCs, in both the fresh and aged organic aerosol. The other significant SOA ion, $C_2H_3O^+$ (m/z 43), appears to be associated with molecules that are more volatile than those responsible for the CO_2^+ fragment. Among the POA ions, the C_xH_y family appears to be less volatile than the $C_{x>1}H_yO_2$ family. Again, this is consistent with the findings of Hennigan et al. (2011) regarding levoglucosan oxidation and the tracer ion m/z 60. The $C_7H_{11}^+$ (m/z 95.086) signal is associated with low-volatility compounds in the fresh POA, a conclusion we draw from the negative signals in Figures 2c and 3. Due to limitations in collision frequency (oxidants and organic compounds), oxidation of organic compounds proceeds much more rapidly when in the gas phase than in the particle phase, even assuming unity reactive uptake of oxidants (Hennigan et al., 2011). It is therefore less likely that the compounds that fragment to $C_7H_{11}^+$ will undergo rapid gas-phase oxidation, and the relative contribution of $C_7H_{11}^+$ to the OA mass spectrum (fC_7H_{11}) will only change due to either heterogeneous oxidation or the condensation of secondary material. We propose to use this ion as a POA tracer ion for biomass burning aerosol in these experiments.

Figure 4 again shows the difference between the fresh and aged OA. However, unlike in Figure 2c, we have scaled the POA mass spectrum by the signal at $C_7H_{11}^+$, shown in equation (3). In equation (3), MS refers to a mass spectrum as an array and $C_7H_{11}^+$ refers to the signal of that individual ion within the array.

$$MS_{Fig\ 4} = MS_{aged} - MS_{fresh} * \frac{C_7H_{11}^+ aged}{C_7H_{11}^+ fresh} \quad (3)$$

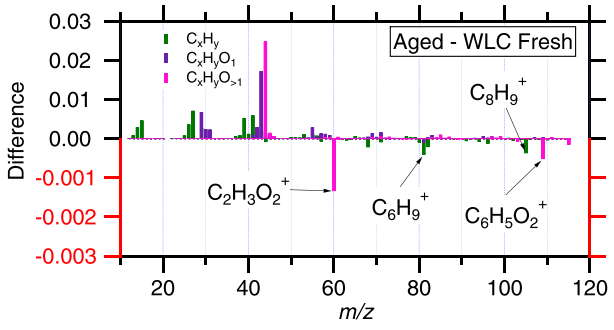

Figure 4. The difference between the aged OA mass spectrum (Figure 2b) and the wall-loss-corrected fresh OA mass spectrum. Wall-loss corrected in this case means the fresh OA mass spectrum (Figure 2a) was scaled by the POA tracer ion, $C_7H_{11}^+$. See equation (3). The positive signal, likely from the SOA, is very similar to other mass spectra for highly oxidized organic aerosol. The negative mass spectrum, shown with a magnified axis in red (1/10th the positive axis), shows small changes in mass for $C_2H_4O_2$, C_6H_9, C_8H_9, and $C_6H_5O_2$.

This allows us to scale MS_{fresh} for changes in signal intensity caused by particle wall loss and changes in collection efficiency due to particle bounce in the AMS. In Figure 4, the signal of $C_7H_{11}^+$ is by definition zero and ions with positive signal likely come from SOA. The SOA includes oxidized ions besides $C_2H_3O^+$ and CO_2^+, consistent with ambient observations of oxidized OA (OOA; Ulbrich et al., 2009). Negative ions are shown on a separate axis in red that is magnified by a factor of 10. These are ions that decrease in signal more than can be accounted for by condensation of SOA, which is accounted for in Figure 4 by normalization to $C_7H_{11}^+$. This shows that in addition to the condensation of SOA, there is potential for the oxidation of intermediate volatility and semivolatile compounds to produce organic compounds that are both more oxidized and potentially more volatile. The signal for ions $C_2H_4O_2^+$, $C_6H_5O_2^+$, $C_6H_9^+$, and $C_8H_9^+$ all decreased more than can be accounted for by the condensation of SOA, particle wall loss, or changes in collection efficiency. However, the change in mass is small, and thus, the POA mass

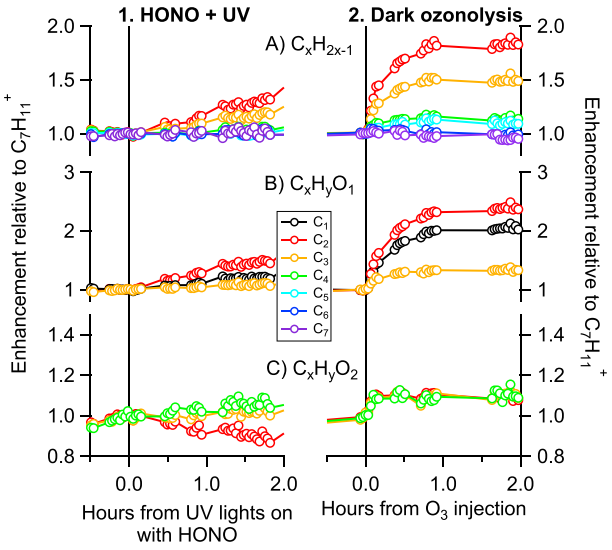

Figure 5. Changes in ion abundance relative to the POA-tracer ion, $C_7H_{11}^+$, before and after two types of simulated aging. Panel series on left shows the oxidation of black spruce smoke in the presence of HONO and UV lights, [OH] = ~2×10^6molec cm^{-3}. Panel series on right shows smoke from the same fire being exposed to ozone (>500 ppb) in the dark. Panel (a) contain ions with the formula C_xH_{2x-1}, panel (b) the formula $C_xH_yO_1$ and panel (c) the formula $C_xH_yO_2$, associated with the semivolatile POA material.

volatilized can be inferred based solely on the ion with the largest negative signal, $C_2H_4O_2^+$ (*m/z* 60).

3.2. Composition Changes Due To Simulated Atmospheric Aging

3.2.1. Specific Ion Changes With Respect to a POA Tracer Ion

The AMS provides both high mass and high time resolution. In order to report changes in OA composition with high time resolution, we correct for particle wall loss and potential changes in particle bounce in the AMS by normalizing ion signals to $C_7H_{11}^+$ (*m/z* 95.086). In Figure 5 we show the relative change in ion abundance during chemical aging of black spruce smoke, with a different panel for each ion family. This figure has two columns for different oxidation conditions and three panels for different ion families. Column 1 shows results for UV illumination after HONO injection, and Column 2 shows results for ozone injection. In each panel we show the changes in the OA mass spectrum for a family, relative to $C_7H_{11}^+$. We further normalize each ion signal fraction (f_i) by its initial value (f_i^t/f_i°), prior to aging. Figure 5a shows the changes in the aliphatic- and aromatic-derived C_xH_{2x-1} fragment ions (typically associated with hydrocarbon-like OA [HOA]) but also present in OOA; Figure 5b shows the changes to the C_xH_yO ions, and Figure 5c shows the changes to the $C_{x>1}H_yO_2$ ions, all relative to $C_7H_{11}^+$.

Figure 5a reveals an increase in C_xH_{2x-1} fragments when $x < 5$ relative to $C_7H_{11}^+$ after both types of aging. If any VOCs are oxidized, resulting in condensation of SOA, those SOA products may fragment to form ions within this C_xH_{2x-1} family where $x <= 5$. However, the ions $C_6H_{11}^+$ and $C_7H_{13}^+$ do not increase relative to $C_7H_{11}^+$. This observation can be explained either by a coincidence of SOA contributing equally and simultaneously to these larger C_xH_{2x-1} ions, or more likely, there was minimal contribution from SOA to any of these ions. Reference spectra for aged organic aerosol, as derived by positive matrix factorization, typically include relatively little signal at higher *m/z* values. For example, for the low-volatility OA factor reported by Docherty et al. (2011), ion signal from all masses above *m/z* 90 comprised less than 3% of the total organic signal, and $C_7H_{11}^+$ contributed only 0.02%. The MILAGRO campaign in Mexico City, a highly oxidizing environment with biomass burning factors identified, showed that very little OOA was $C_7H_{11}^+$, ~2×10^{-6}% (Aiken et al., 2009). Thus, we believe that there is little SOA contribution to $C_7H_{11}^+$ in these experiments (Ulbrich et al., 2009).

Figure 5b shows the change in the singly oxygenated ions ($C_xH_yO^+$) relative to $C_7H_{11}^+$. Both oxidation conditions result in enhancement of CHO^+, $C_2H_3O^+$, and $C_3H_5O^+$. The experiment with OH aging from added HONO, [OH] = ~2×10^6molec cm^{-3}, shows a more gradual increase in the oxidized species compared to the ozone aging experiment; this is consistent with the trends observed for known SOA production from precursors such as monoterpenes. For ozone experiments, $[O_3] > 500$ ppb, the monoterpene signal decreases rapidly upon ozone injection, whereas for OH oxidation experiments the decrease is more gradual (Atkinson & Arey, 2003; Presto & Donahue, 2006).

Figure 5c shows the change in ions with two oxygen atoms ($C_{x>1}H_yO_2^+$) relative to $C_7H_{11}^+$. Figure 2c shows that the ions of $C_{x>1}H_yO_2^+$ are predominantly POA despite their high oxygen content and also that they are more volatile than the compounds that resulted in C_xH_{2x-1} ions. Ozonolysis results in a modest enhancement of the $C_xH_yO_2$ family, likely due to SOA formation as organic acids (Fortenberry et al., 2018). This is also consistent with the findings of Ortega et al. (2013), who observed enhancement of these ions using a photooxidation flow reactor to age biomass burning emissions. However, in the HONO + UV experiment the ratio of $C_2H_4O_2^+$ to $C_7H_{11}^+$ decreases. This is consistent with the findings of Hennigan et al. (2010, 2011), who showed that levoglucosan does react via gas-phase oxidation. This reduces the partial pressure of levoglucosan over the particle surface, which in turn drives particulate levoglucosan to the gas phase to reestablish equilibrium. If we assume that all wall-loss-corrected $C_2H_4O_2^+$ depletion is due to the loss of levoglucosan, we can estimate a lower limit of the fraction of POA evaporated via levoglucosan

volatilization by using the reference spectrum of pure levoglucosan. This estimate of POA evaporation does not include mass volatilized due to the dilution of the smoke into the smog chamber, but it is more representative of POA evaporation and atmospheric processing after the smoke has already undergone significant dilution with background air. Thus, the fraction of wall-loss-corrected POA that is volatilized and oxidized as levoglucosan at time t is shown in equation (4) as

$$fPOA_{levo-vol} = \left(C_2H_4O_2^+ init - C_2H_4O_2^+ t \frac{C_7H_{11}^+ init}{C_7H_{11}^+ t}\right) * \frac{1}{f_{C_2H_4O_2^+ levo} * Org_{init}} \quad (4)$$

where Org_{init} is the AMS-measured organic mass at 0 hr, $C_xH_yO_z^+$ are ion signals at 0 or 1.5 hr, and $fC_2H_3O_2^+{}_{levo}$ is the fraction of a levoglucosan reference mass spectrum that comes from $C_2H_3O_2^+$. Though $C_2H_4O_2^+$ (m/z 60) is one of the more volatile ions in Figure 5, this does not exclude evaporation of other semivolatile POA components. However, the signals for the larger $C_xH_yO_2^+$ ions follow the same trend as $C_7H_{11}^+$, and thus, the ratio stays constant (Figure 5). This suggests that for these experiments, the compounds contributing to these fragment ions are effectively nonvolatile, or conceivably that there is equivalent simultaneous production and loss of these compounds (we regard this as unlikely).

3.2.2. Changes in Characteristic AMS Tracer Ions

The ratio of characteristic AMS fragments to the total OA spectrum (expressed as $f_{m/z}$) provides a useful comparison against ambient observations. Such ratios are plotted in Figures 6a and 6b. The magenta symbols indicate fresh emissions, and the cyan symbols indicate the combined primary and secondary OA after aging, and each pair of fresh and aged points is tied with a line segment. Closed symbols are coniferous canopy fuels (i.e., black spruce and ponderosa pine), and open symbols are other fuels (e.g., grasses and peat). In Figure 6a, we plot f_{44} (mostly CO_2^+) against f_{43} ($C_3H_7^+$ and $C_2H_3O^+$). A zoomed in version is included in the Supporting Information, Figure S3. The triangle indicates the portion of this space observed by Ng et al. (2010) that encompasses most ambient OA. The ambient triangle shows that fresh emissions have a range of f_{43} values and relatively low f_{44}; with increased atmospheric aging, ambient f_{44} approaches a maximum of 0.3, and f_{43} converges to 0.035. We include the data from the Hennigan et al. (2011) FLAME-III study of aged biomass burning aerosol, with fresh OA plotted as black crosses and aged OA plotted as blue circles. Consistent with the OA from FLAME-III, our smoke has low f_{43}, though it is somewhat higher than reported by Hennigan et al. Our fresh smoke also has low f_{44}, especially for the coniferous canopy fuels (i.e., black spruce and ponderosa pine). The grasses have a higher initial f_{44}, around 0.06. Peat smoke has a relatively low f_{44}, similar to that of coniferous-canopy smoke.

After oxidation, we observed an increase in both f_{44} and f_{43}. However, because we did not age our aerosol as long or as extensively as Hennigan et al. (2011), the f_{44} values of our aged smoke also did not reach as high. Note that ozonolysis experiments, with their high concentration of oxidants, formed significantly more total organic mass (shown below in Figure 9) and thus increase significantly in both f_{44} and f_{43} (Tkacik et al., 2017). In contrast, OH oxidation driven by the UV lights and HONO photolysis increases f_{44} relatively more, and the slope of the OH oxidation experiments (triangles and squares) in Figure 6a reflects this.

In Figure 6b we plot the OOA tracer f_{44} against the biomass burning tracer f_{60} (Cubison et al., 2011; Hennigan et al., 2011). Coniferous-canopy fuels produced a wide range of initial f_{60} values. Although we conducted replicate burns of similar fuels, even those show a wide range of initial f_{60} values. POA from coniferous-canopy fuels spans a range from 0.005 to 0.03 in initial f_{60}, suggesting that fire-to-fire variability is more important than the fuel with respect to initial f_{60} values. However, in all cases, aging of biomass burning OA causes f_{44} to increase and f_{60} to decrease. This was most pronounced when significant SOA was formed, although dark control experiments also revealed a small decrease in f_{60} as well, less than 0.002. This was potentially due to absorption of gas-phase levoglucosan into the Teflon chamber walls, which would promote further evaporation of POA.

3.3. Determining the SOA Mass Produced During an Aging Experiment

We have already seen that the aging experiments resulted in SOA formation with a mass spectrum displaying characteristic SOA ions (Figure 2c). Next, we estimate the absolute production of SOA mass. This requires quantification of SOA condensation to two reservoirs—suspended particles and the wall region

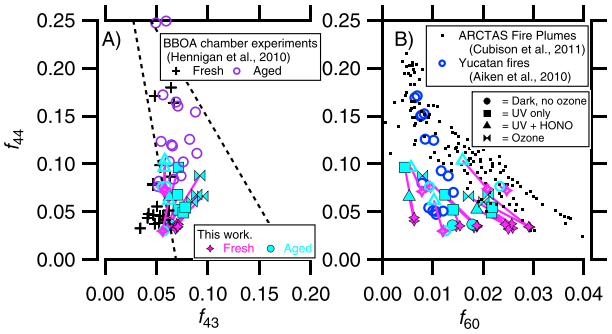

Figure 6. The ratio of certain AMS OA ion fragments to the total organic aerosol ion signal (f_i) provide a useful comparison against ambient observations (dashed lines). In both panels, magenta symbols indicate emission prior to oxidation, and cyan indicates the OA after aging. Closed symbols are coniferous canopy fuels (i.e., black spruce and ponderosa pine), and the open symbols are the other fuels (e.g., grasses and peat). In panel (a) f_{44} (OOA marker) is plotted against f_{43} (less oxidized). Consistent with Hennigan et al. (purple circles are aged experiments, black crosses are fresh emissions), the initial burns have relatively little f_{43} or f_{44}, but increase in both as a result of oxidation (Hennigan et al., 2011). In panel (b) the OOA tracer f_{44} is plotted against the typical biomass burning tracer f_{60}. Measurements of ambient biomass burning plumes are shown for comparison. Data from Cubison et al. (2011) is shown as black dots and the data from Aiken et al. (2010) are shown as blue circles.

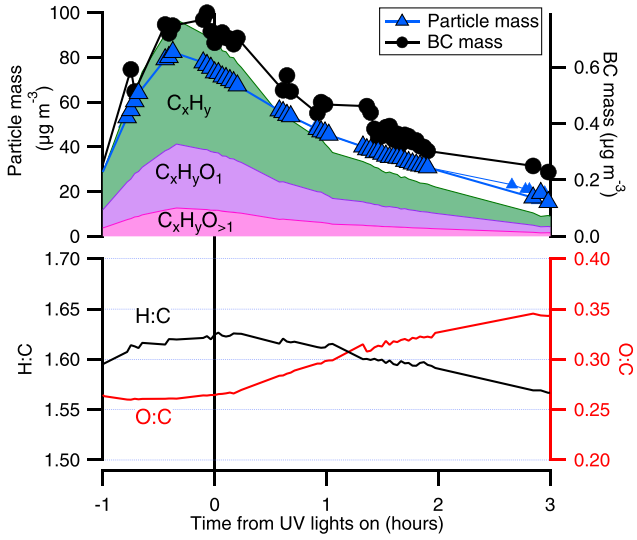

Figure 7. Particle mass and composition measurements during a typical BBOA aging experiment. Smoke from black spruce was aged using UV lights with no added oxidant (157-1 from Table 1). Total particle mass (blue triangles) is calculated from the particle volume determined by the SMPS assuming a density of 1.3 g/cm^3. Black carbon (black circles) was measured by the SP2. AMS measurements of particle organic carbon mass and OA chemical families are the solid filled traces. The H:C and O:C elemental ratios of the OA derived from the AMS measurements are plotted in the lower panel.

(either to wall-deposited particles or to the Teflon itself)—and also the deposition of suspended SOA particulate mass to the walls. The process is conceptually straightforward but technically challenging (Bian et al., 2015; Matsunaga & Ziemann, 2010; Trump et al., 2016; Ye et al., 2016; Zhang et al., 2014). It involves first quantifying the evolution of the total suspended OA mass concentration and then attributing the changes in OA concentration between net condensation and the various wall-loss mechanisms. All measurements of the suspended OA concentration suffer from systematic uncertainties (e.g., unknown particle mixing state or morphology), which are amplified when determining differences; however, as described below, the aerosol composition measurements provided by the AMS can be exploited to alleviate these effects.

Figure 7 shows mass and composition measurements of a typical biomass burning aerosol aging experiment. After we start to inject the smoke at $t = -1.0$ hr, the BC mass concentration measured by the SP2 increases. After injection is complete, the BC mass decreases as particles are lost to the walls. The particle volume measured by the SMPS follows the same general trend. Using particle mobility diameter (from SMPS) and vacuum aerodynamic diameter (from AMS), one can calculate the average effective particle density (DeCarlo et al., 2004; Jayne et al., 2000). We use this measured average effective density for our sampled particles, ~1.3 g/cm^3, to convert SMPS-determined integrated particle volume into total particle mass. The AMS-measured organic mass, separated into ion families as previously discussed, is also shown in Figure 7 and follows the same general trend. Since the particle mass is mostly nonrefractory organic material (BC < 10% of total mass), one might expect a closer correlation between SMPS-measured particle mass and AMS-measured mass. However, although biomass burning POA is typically assumed not to bounce off the AMS vaporizer (collection efficiency = 1.0), smog-chamber SOA and ambient OOA typically have been reported to experience particle bounce, resulting in a collection efficiency as low as 0.3 (Docherty et al., 2013; Robinson et al., 2017). In this work, we assume that fresh biomass burning aerosol has unit collection efficiency; this assumes that there is no compositional bias due to an undersampling of bouncy (CE < 1) particles. Furthermore, the aged particles exhibit a collection efficiency <1 due to the condensation of SOA, a process to which the particles are all subjected. If we assume that the particles are coated with SOA simultaneously, the resulting reduction in collection efficiency is not likely to induce an undersampling of a specific type of particle. In these experiments, we are assuming that there is no compositional bias to initial measurements (CE = 1) and that the SOA products are of sufficiently low volatility that they condense on particles independent of composition. Therefore, the changing collection efficiency as a result of SOA condensation does not change *which* particles are sampled, only *how many* of them, and so the composition measurements can be considered as independent of collection efficiency. Thus, the relative contribution of the POA tracer ion $C_7H_{11}^+$ to the total organic signal can be used to calculate the SOA mass produced, POA mass volatilized, and therefore total OA enhancement.

We use the low-volatility, primary organic ion $C_7H_{11}^+$ tracer as an internal standard for POA within the AMS mass spectrum (Hennigan et al., 2010; Heringa et al., 2011). The use of an internal standard allows us to calculate OA enhancement, SOA mass, and POA mass with greater precision than would be possible using a single assumed collection

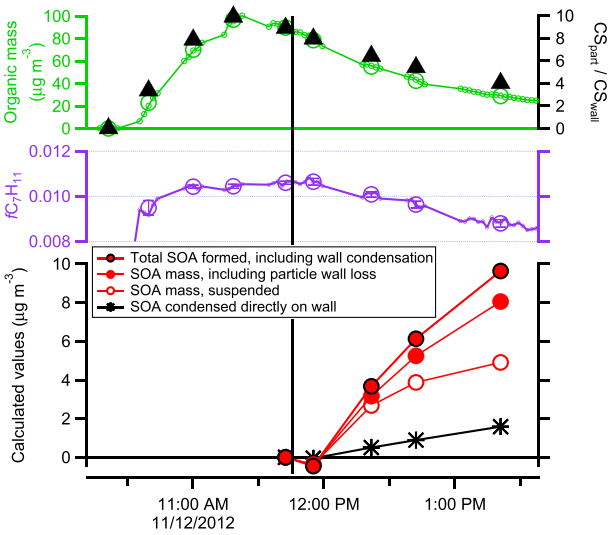

Figure 8. Measured and calculated values required for estimating the total SOA produced by accounting for SOA mass that is lost to the walls either by condensing directly or by deposition as a particle. The experiment shown as an example is the photooxidation of black spruce smoke (157-1 from Table 1). The top panel shows that injecting smoke causes an increase in organic aerosol (green circles), and also an increase in the ratio of the suspended condensation sink and the Teflon walls condensation sink (black triangles). The middle panel shows the evolution of the mass spectra, represented as the fraction of organic signal contributed by the ion $C_7H_{11}^+$, f_{C7H11}. Once aging begins and SOA condenses (black vertical line), f_{C7H11} decreases. The final plot on the bottom shows the evolution of the SOA with time, described in section 3.3.

efficiency. The use of $C_7H_{11}^+$ as a POA tracer ion is based on the implicit assumption that the OA composition is homogeneous (i.e., f_{C7H11} is independent of particle size and the particles are internally mixed) and that heterogeneous oxidation of the particles is slow. The consistent ratio of $C_7H_{11}^+$ with the large C_xH_{2x-1} ($x > 5$) ions supports the assumption that any contribution to $C_7H_{11}^+$ from SOA is negligible or consistent across these fragments (Figure 5a). The precision gained from removing the uncertainty in variable AMS collection efficiencies is larger than the uncertainties associated with the assumption that the particles are homogeneous and heterogeneous oxidation is slow. In Supporting Information Figure S1, we compare the OA enhancement factors calculated using both methods: the ratio of SMPS-measured particle mass to BC and the relative contribution of $C_7H_{11}^+$ to the total organic signal, f_{C7H11+}. While both methods give similar results, the precision of the OA composition-based method of calculating OA is generally much better than the SMPS-based method.

With a POA tracer ion, we can estimate the relative amount of SOA condensed on the particles during an experiment. However, we must also account for any SOA that condensed directly onto the smog chamber walls. For each chamber experiment, we averaged data for each 5-min interval defined by the sampling valve switching period between the two smog chambers. We show an example of the SOA calculation in Figure 8. We calculate the amount of SOA condensed onto the remaining suspended particles for each interval based on the composition change. The change in the amount of SOA on the particles is defined in equation (5):

$$d\mathrm{SOA}_{\mathrm{particles}} = \left(\frac{\mathrm{Org}(t) + \mathrm{Org}\,(t-1)}{2}\right) * \left(\left(1 - \frac{f_{C_7H_{11}}(t)}{f_{C_7H_{11}}(\mathrm{init})}\right) - \left(1 - \frac{f_{C_7H_{11}}(t-1)}{f_{C_7H_{11}}(\mathrm{init})}\right)\right) \quad (5)$$

where $d\mathrm{SOA}_{\mathrm{particles}}$ is the change in the amount of suspended SOA from time t relative to $t-1$ and Org is the OA mass concentration ($\mu g/m^3$). The term $f_{C7H11}(\mathrm{init})$ indicates the initial contribution of $C_7H_{11}^+$ to the total OA signal, prior to aging, while $f_{C7H11}(t)$ and $f_{C7H11}(t-1)$ are its contribution at those two respective times. The integral of $d\mathrm{SOA}_{\mathrm{particles}}$ is the total amount of SOA condensed on the particles, including particle wall loss. If we were to neglect vapor condensation directly to the walls, this correction would conclude the calculation; it is thus a lower limit to the total SOA production. This set of assumptions is referred to as the $\omega = 0$ case in earlier work (Hennigan et al., 2011; Weitkamp et al., 2007), where ω is the proportionality factor that describes the ability of vapors to partition to OA on the walls and to suspended particles. When $\omega = 0$, condensable products only partition to suspended particles. When there is perfect equilibrium between the bulk phase and the particles on the wall, $\omega = 1$ (Weitkamp et al., 2007).

To estimate the amount of SOA that condensed directly to the walls, without considering any deposited particle mass, we first need to know the collision frequency of vapors with the walls and with the suspended particles. We then calculate the loss frequency (the condensation sink) to each of those two reservoirs and assume that the condensation fluxes are proportional to those condensation sinks. This is accurate in the limit when the condensing vapors are effectively nonvolatile, meaning that the saturation ratios are very high (Donahue, Trump, et al., 2011; Trump et al., 2016). For the Teflon walls, independent of any deposited aerosol mass, we assume that the condensation sink is the collision frequency and that the deposition is effectively irreversible, consistent with observations of semivolatile organics (Krechmer et al., 2016; Ye et al., 2016). For these chambers, based on the surface to volume ratio, that gives a wall condensation sink of 1/8 min^{-1} (McMurry & Grosjean, 1985). For the suspended particles, we need to know the Fuchs corrected surface area, modified by the normal vapor speed and the mass accommodation coefficient (Saleh, Hennigan, et al., 2013; Seinfeld & Pandis, 1998). After we stop injecting smoke and begin oxidation, the Fuchs-corrected surface area increases as the particles grow but decreases as the particles diffuse to the

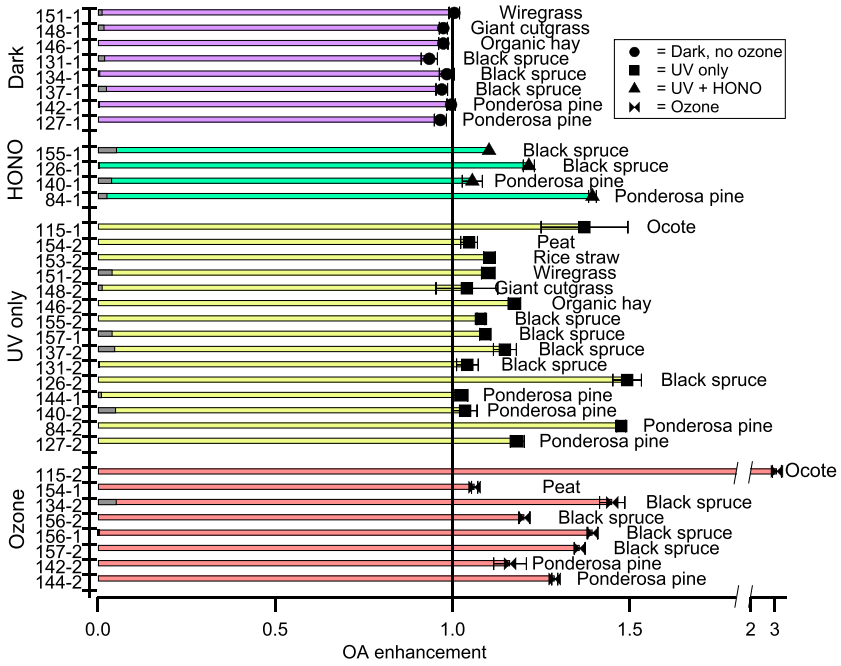

Figure 9. Calculated OA enhancements are plotted versus the FLAME-IV burn number (left column), and then the smog chamber number (#-1 or #-2). Error bars indicate the standard error. OA enhancements are grouped by the perturbation type, and then by fuel types. Nonconiferous canopy fuels are plotted first, and then black spruce, and ponderosa pine. We calculated SOA formation using the decrease in $fC_7H_{11}^+$ as an indicator of new material condensing on the POA. We also used the decrease in $C_2H_4O_2^+$ relative to $C_7H_{11}^+$ to estimate the mass of levoglucosan that evaporated from the particles. This is shown as a fraction of the initial OA mass as a gray bar in the column; this does not exclude other POA evaporation.

walls. We use the method described in Sinha et al. (2017), who found a mass accommodation coefficient of 0.3 for particles in FLAME-IV. We then calculate the mass of SOA condensation directly on the walls:

$$d\mathrm{SOA}_{\mathrm{walls}} = d\mathrm{SOA}_{\mathrm{particles}} * \frac{\mathrm{CS}_{\mathrm{walls}}}{\mathrm{CS}_{\mathrm{particles}}} \quad (6)$$

Equation (6) shows that when the condensation sink of the suspended particles is high, the SOA lost to the walls is small relative to the total SOA produced. The average ratio of the condensation sink for suspended particles to the condensation sink of the Teflon walls for our experiments was 5, and thus, the correction of vapors lost to the walls is small, typically 15% or less of $d\mathrm{SOA}_{\mathrm{particles}}$.

We obtain an upper limit for SOA produced by assuming that particles deposited to the walls remain in equilibrium with the suspended particles via gas-phase partitioning (the $\omega = 1$ case). We show this correction with blue markers in Figure 10, which is a comparison between measured and modeled SOA, discussed below. In this scenario, particles that have deposited on the wall grow as much as the observed particles that are still suspended. This assumption can increase the calculated SOA by about a factor of 2.

With the wall condensation constrained, the sum of the SOA on the walls and the SOA condensed on the particles represents the total SOA formed from the oxidized VOCs in the smog chamber. We show contributions to each reservoir in Figure 8 for the $\omega = 0$ case. It should also be noted that for these experiments a minimal amount of time (~15–45 min) was allowed between filling the chamber and perturbing it. This was to reduce the amount of semivolatile vapors that would be absorbed into the Teflon walls.

3.4. OA Enhancement From Various Fuels and Perturbations

In Figure 9 we show the calculated OA enhancements for all the chamber experiments after 1.5 hr of aging. We calculated the OA enhancements using equation (7):

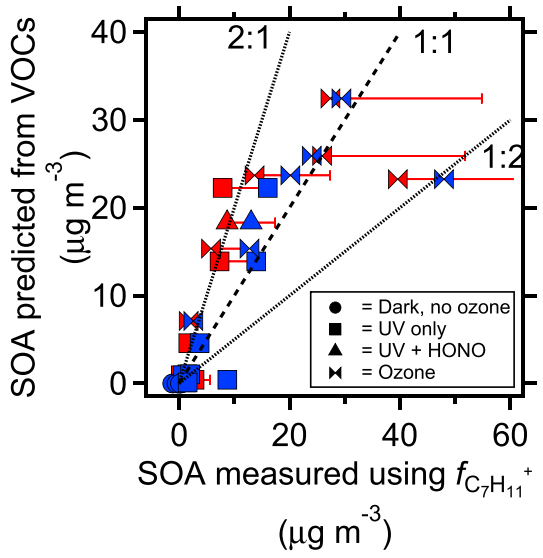

Figure 10. SOA mass predicted using speciated and scaled VOC measurements is plotted versus SOA mass observed in AMS measurements using the $C_7H_{11}^+$ (m/z 95.086) POA tracer. Blue symbols indicate SOA mass calculated assuming that particles on the wall are in equilibrium with the suspended particles. Red symbols indicate SOA mass calculated assuming an irreversible condensation sink on the wall of 1/8 min^{-1}. The error bars on the red points indicate the SOA mass that would result from assuming that after SOA condenses on the particle, the probability of a particle bouncing off the AMS vaporizer goes from 0 to 50%. Symbol shapes indicate the aging perturbation used in that experiment.

$$\text{OAenhancement} = \left(\frac{\text{SOA} + \text{POA}}{\text{POA}}\right) \quad (7)$$

Dark control experiments, where we injected the smoke into both smog chambers and then imposed no perturbation on one chamber, show very little change in OA enhancement, on average OA enhancement = 0.998 with a standard deviation of 6%. Consistent with what was observed in Figure 6 for f_{60}, there may be a small decrease in OA mass that is potentially within the precision of the method. Gray bars on the left of the OA enhancement indicate the calculated mass that would volatilize if the decrease in f_{60} was due to the volatilization of levoglucosan. This may explain some of the decreased OA enhancements for dark experiments. Broadly, the very small changes to the dark control experiments confirm the method and also the value of our dual-chamber experiments, as the null reference is available to compare the perturbed experiment to, for the same smoke simultaneously injected into both chambers (Tkacik et al., 2017). We show the calculated mass of volatilized levoglucosan as a fraction of the initial OA mass as gray bars in Figure 6 for t = 1.5 hr. In all cases, the calculated mass loss due to evaporation of levoglucosan was less than 5% of the initial OA in dilute smoke, though presumably other species without fragments at m/z 60 contribute to POA evaporation as well.

For HONO and UV experiments where OH radicals were used to age the biomass burning aerosol from similar fuel sources, we observed a modest OA enhancement, 1.17 ± 0.15, consistent with the condensation of SOA (Tkacik et al., 2017). Within experiments for a given fuel type (e.g., ponderosa pine) and the same perturbation (UV, HONO, or O_3) the enhancement was highly variable, again confirming the importance of burn-to-burn variability. On average, experiments where ozone was added had a higher OA enhancement, 1.48 ± 0.67. One ozone experiment where ocote was burned had a very high OA enhancement, close to 3. This was largely driven by the fact that very little initial OA was injected into the chamber (see Table 1 and the Supportin Information discussion). In the presence of >500 ppb of ozone, 66% of the measured monoterpene concentration had reacted after 1.5 hr. For an OH oxidation experiment, it took 3.8 hr to react away 66% of the measured monoterpenes. Thus, for the ozone experiments, we would expect that more ozone-reactive SOA precursors would have been oxidized after 1.5 hr, producing the larger OA enhancement.

While on average these OA enhancements are smaller than those reported by Hennigan et al. (2011) from FLAME-III (1.7 ± 0.7), this is consistent with the lesser extent of aging employed during our FLAME-IV experiments that used a shorter total aging time to reduce the effects of wall losses. This is consistent with the lower $f44$ and $f43$ values for these experiments compared to those of Hennigan et al. (2011), shown in Figure 6. In Figure 2 from Hennigan et al. (2011), an SOA formation time series is shown to end after 4 hr with an OA enhancement of ~2.8, one of the higher OA enhancements reported in that work. At a time comparable to those used in this work, 1.5 hr, Figure 2 from Hennigan et al. (2011) shows an OA enhancement of ~1.5, similar to the high OA enhancements reported in this work for a similar aging time. The OA enhancements reported in this work are on average 18% lower than OA enhancements reported in Tkacik et al. (2017) for the same smog chamber experiments. This is because Tkacik et al. (2017) used later end points when possible. We selected the shorter aging period for this work to allow the comparison of gas- and particle-phase data, some of which are not available for the full duration of each experiment. The OA enhancements reported by Hennigan et al. (2011) were at the end of the experiments, after roughly 5 hr of oxidation with an average OH concentration of ~0.2–1 × 10^7molecules cm^{-3}. Our measurements report the state of aging after ~1.5 hr at similar OH concentrations. In some cases, another fire was started in the same room as our smog chambers, which was readily detected as a contamination source in our chambers. We discarded any contaminated data; all plots indicating *after aging* refer to ~1.5 hr of aging for consistency.

3.5. Predicting the Amount of SOA Formed

Biomass combustion produces abundant VOC emissions in addition to POA. Some of these VOCs are the result of incomplete combustion (e.g., benzene and toluene), and some are present in the fuel itself and volatilized by the heat of combustion, but otherwise unaltered (e.g., terpenoids; Hays et al., 2002; Reid et al., 2005; Schauer et al., 2001). Regardless of their origin, some of these VOCs can be oxidized to produce SOA. Emissions of unburnt VOCs are significantly higher from folial mass and green wood than from dried firewood (Stockwell et al., 2015). Hatch et al. (2015) reported the composition and abundance of over 400 volatile organic compounds for four of the fuels we used for our aging experiments, based on GC × GC-TOFMS analysis of cartridge samples from FLAME-IV.

We observed that absolute emissions from a given fuel type varied from burn to burn, but the relative composition of different vapors—the fingerprint of a given fuel type—was more stable (e.g., Figure S2 in Hatch et al. (2015)). Our actual burn conditions for a given fuel type were consistent with respect to ignition and staging. For this reason we used a tracer molecule that we could measure accurately and precisely in each smog chamber with the real-time PTR-MS and estimated the full emissions based on the average emission fingerprint measured via offline.

Here we use toluene as the tracer for a given burn because it can be measured precisely with the PTR-MS and analysis of the offline GC × GC-TOFMS samples showed that there were no significant interfering isomers that would interfere with the PTR-MS measurements of toluene. Broadly, we can divide the VOC emissions into intrinsic compounds present in the fuel in the first place that are volatilized during the burn, including monoterpenes, but also derived compounds such as toluene that are likely pyrolysis products of the combustion. It is possible that the emissions from these two classes depend differently on burn conditions. Although we controlled those conditions carefully, differences in combustion temperatures and rates may shift the ratio of pyrogenic versus biogenic VOCs between fires in this work and likely will shift them in less controlled conditions. Therefore, we do not recommend using toluene as a general tracer for VOC emissions from biomass combustion.

Here we will assume that the composition of the volatile emissions from a given fuel—the set of concentration ratios—is more stable for any given fuel type than the absolute emissions, given that our burn protocol was consistent. We will thus use the average composition from Hatch et al. (2015) as the emission profile for a given fuel type and normalize that to the initial toluene measured in our PTR-MS for a given experiment. This allows us to estimate the speciated, initial VOC mass present in the smog chambers for each experiments.

We also use the PTR-MS measurement of toluene to estimate the OH exposure after perturbation (equation (1); Hennigan et al., 2011; Heringa et al., 2011) for each smog chamber experiment. To estimate the amount of SOA produced by a VOC for each experiment—the sum of which will be the total SOA production—we must know the SOA yield and the reaction rate constants with OH. For some of the VOCs quantified by Hatch et al., we can use the literature value from Atkinson and Arey (2003). For others, we follow the suggestions of Hatch et al. (2015), who proposed estimates based on structural and functional similarities with VOCs found in the literature. The SOA yield for each VOC is established similarly with an important caveat: SOA is assumed to be nonvolatile. This is a large source of potential error in the SOA estimation. For example, the effective SOA yield of α-pinene oxidation can vary from 0.07 to 0.3 as a result the volatility distribution of its oxidation products and the OA mass concentration (Presto et al., 2005; Presto & Donahue, 2006). NO_x can also affect the volatility distribution of SOA products (Kari et al., 2017; Presto et al., 2005). Neither of these effects are considered in this analysis; we use a simple effective SOA yield parameter where the product of VOC mass reacted and SOA yield is equal to the SOA produced. Similarly, representative SOA yields reaction rate constants were applied to the compounds in the emission inventory of Hatch et al. (2015). While a more accurate accounting of physical constants would certainly be beneficial, these assumptions serve to show fairly good agreement between predicted and measured SOA. The full table of representative rate constants and assumed yields from Hatch et al. (2015) and used in this work is available in Table S2.

In summary, we calculated OH exposure from the decay of toluene for each experiment. We then scaled the fuel-dependent emission profile from Hatch et al. (2015) by the initial toluene concentration measured in each smog chamber and then calculated the amount reacted using literature rate constants and best

estimates. Finally, we multiplied the mass of VOC reacted by a scalar SOA yield, which is assumed to be independent of chemistry or product volatility. That mass divided by initial OA measured at the beginning of the experiment is the predicted SOA yield for each OH aging experiment.

For ozonolysis experiments, we assumed compounds with carbon-carbon double bonds (principally monoterpenes) were all oxidized. One important caveat of this method is the relatively slow reaction of terminal double bonds, present in two of the 10 monoterpenes measured in these emissions. This terminal carbon double bond reacts ~30 times slower with ozone than an internal double carbon bond (Atkinson & Arey, 2003). For black-spruce emissions, camphene, which has a terminal carbon double bond, constitutes roughly 30% of the monoterpenes measured. PTR-MS measurements show that for ozonolysis experiments, the total monoterpene signal decreases rapidly before seeming to plateau at 30% of the initial signal, whereas our simplified model of the ozonolysis experiments predicts no monoterpene signal should remain. As pointed out by Hatch et al. (2017), this may also be due to the presence of other VOCs, which are detected in the PTR-MS at m/z 137, that is, bornyl acetate. Bornyl acetate was observed in black-spruce emissions by GC × GC-TOFMS and is effectively nonreactive toward ozone (Hatfield & Huff Hartz, 2011).

3.5.1. Comparing Mass of SOA Formed to Mass of SOA Expected From VOC Oxidation

In Figure 10 we compare the predicted and measured SOA mass for the various biomass burning smog-chamber experiments. We show the measured SOA for the $\omega = 1$ scenario (blue) and the $\omega = 0$ case with the wall-loss correction described in section 3.3 (red). The error bars on the red markers indicate the possible SOA mass measured for a range of AMS collection efficiencies between 1 (our best guess, shown as the marker) and 0.5 (the lower limit, shown as the error bar). The predicted SOA agrees to within about a factor of 2 of the estimated SOA. For the SOA prediction scenario with the highest yield, $\omega = 1$, the predicted SOA mass is on average 67% higher than the observed SOA. However, the uncertainty in the AMS collection efficiency spans the 1:1 line between measured and predicted SOA. Further, although biogenic emission profiles may be similar for the same fuel from burn to burn, the ratio of pyrogenic versus evaporative, biogenic emissions may vary widely from fire to fire (Tkacik et al., 2017). Consequently, our scaling of emission factors based on measured toluene is likely uncertain to at least a factor of 2.

The modest overprediction is especially interesting given that some lower volatility compounds were biased low in the Hatch et al. (2015) inventory (Hatch et al., 2017). Although the dual adsorbents in the adsorption-thermal desorption cartridges used to generate the VOC inventory enable collection of organic gases with a broad range of volatilities, a multi-instrument comparison indicates that the desorption cartridges may have undersampled oxygenated species (Hatch et al., 2017). These oxygenated species constitute the majority of intermediate volatility organic compounds (IVOCs) present in biomass burning emissions (Hatch et al., 2017). IVOCs have a saturation concentration, C^*, between 300 and 10^6 $\mu g/m^3$ (e.g., alkanes C_{12}–C_{22} and polyaromatic hydrocarbons with three or four rings) and are thought to contribute significantly to SOA formation in petroleum combustion emissions (Donahue et al., 2012; Presto et al., 2009; Zhao et al., 2014). Although the oxygenated IVOCs may not have been accurately measured, we show that the VOC inventory presented in Hatch et al. (2015) allows for prediction of SOA formation in our smog-chamber experiments to within a factor of 2. This good agreement using a VOC inventory that underestimates IVOC-generated SOA can be explained two ways. The IVOCs may have produced relatively little SOA mass, or they may have been lost during smoke transfer to the smog chambers, despite the heated, chemically passivated, and smoke-conditioned transfer lines (Tkacik et al., 2017).

In either case, the majority of the SOA mass in these experiments, and similar smog-chamber experiments using biomass burning emissions from undried fuels still containing abundant volatiles such as terpenes, can be explained by the measured VOC SOA precursors. For grasses and agricultural cuttings where less well-studied VOC precursors (e.g., furans) were the prevalent source of SOA, less than 5 $\mu g/m^3$ SOA mass was predicted or measured (Table 1). Low OA mass loadings in these experiments may minimize the effect of the poorly constrained SOA yield of these compounds (Hatch et al., 2017).

The variability in the biomass burning OA enhancements between burns in these experiments can largely be explained by variability in those precursors rather than necessitating the inclusion of unmeasured species such as intermediate volatility organic compounds (IVOCs; Grieshop, Donahue, & Robinson, 2009; Zhao et al., 2014). The variability ultimately relates to burn conditions and fuels. However, the uncertainty in the model-

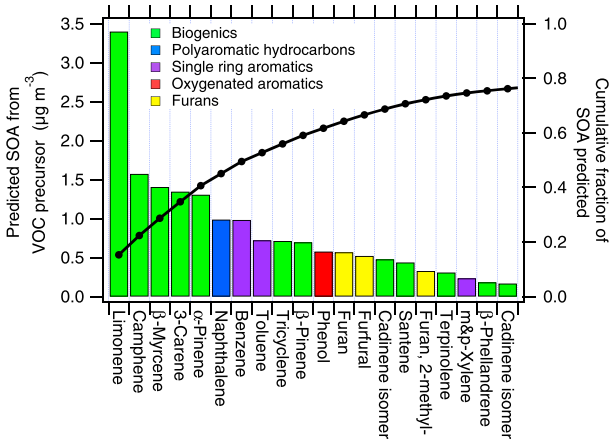

Figure 11. Predicted SOA mass using speciated VOC measurements, following the aging of black spruce smoke by OH oxidation. The colored bars show the absolute SOA mass. The right axis (black circles) shows the fraction of the cumulative SOA predicted to be formed, ~20 μg/m^3. Although only twenty VOC species are shown on the plot, over 400 total species were identified and quantified by Hatch et al. (2015).

measurement comparison is at least a factor of 2, and so we cannot rule out a significant role for IVOC oxidation in the total SOA formation.

3.5.2. Fuel-Dependent Sources of SOA

3.5.2.1. Coniferous Canopy Fuels

We show the predicted SOA mass contribution of individual VOCs from a black-spruce smoke aging experiment in Figure 11. The precursors are colored by their chemical class. Biogenic compounds (mostly terpenoids) are green, polycyclic aromatic hydrocarbons are blue, branched aromatics are purple, oxygenated aromatics (including phenol and guaiacol) are red, and furans are yellow. The black traces show the same data but as a cumulative fraction, plotted on the right axis. More than 40% of the SOA produced is predicted to come from oxidation of monoterpenes. This stands in contrast to aging experiments by Bruns et al. (2016) and Tiitta et al. (2016) using dried logwood smoke from a residential woodstove. They observed good agreement between measured SOA mass and predictions based on the oxidation of mostly pyrogenic VOCs, that is, benzene, naphthalene, and toluene. Tiitta et al. (2016) and Bruns et al. (2016) studied a more controlled form of combustion and burned only dried hardwood, and they did not observe any monoterpene emissions. In our experiments with coniferous canopy fuels (e.g., black spruce and ponderosa pine) we burned freshly harvested whole branches with foliage. The mass of the branches was dominated by needles with comparatively little mass of bark or wood in the twigs. In addition, in nearly every experiment, the needles dominated actual fuel consumption and the branches were minimally burned. For these fire conditions, which may be representative of some crown fires, the emissions from monoterpenes are critical for predicting the SOA formation potential.

The GC × GC-TOFMS measurements of the smoke emissions allowed Hatch et al. (2015) to identify dozens of individual monoterpenes. In contrast, other experiments measuring monoterpenes using only PTR-MS measurements cannot rule out other species producing signal at m/z 137 (i.e., bornyl acetate) and must make assumptions about monoterpene speciation, which affects their reactivity with OH and O_3 and their SOA yields. Grieshop, Logue, et al. (2009) represented all of the monoterpenes as α-pinene. We assessed this simplification by comparing the SOA predicted from our speciated measurements with the SOA predicted when representing all of the monoterpenes as α-pinene. Our detailed model predicts that α-pinene is responsible for less than one quarter of the monoterpene-derived SOA; however, the net error caused by representing all monoterpenes as α-pinene is relatively small, supporting the approach of Grieshop, Logue, et al. (2009), especially for fires with needle-rich fuels. For the OH oxidation experiments, the simplified model gives 6% less SOA mass than the fully speciated model that uses the GC × GC-TOFMS measurements as emission profiles for each fuel. For the ozonolysis experiments, the simplified model gives 15% more SOA mass.

The speciation was important however for explaining temporal trends in unspeciated monoterpene signal measured by the PTR-MS at m/z 137. In cases such as black-spruce-derived smoke, where less reactive monoterpenes (e.g., camphene) or bornyl acetate were abundant, the m/z 137 signal decayed more slowly than one would expect if all the signal at m/z 137 was from α-pinene (Atkinson & Arey, 2003; Hatch et al., 2017). Thus, the effectiveness of calculating SOA production assuming that PTR-MS measured signal at m/z 137 is from α-pinene is an example of cancelation of errors. The validity of this assumption needs to be tested across a more comprehensive sample of biomass burning emissions.

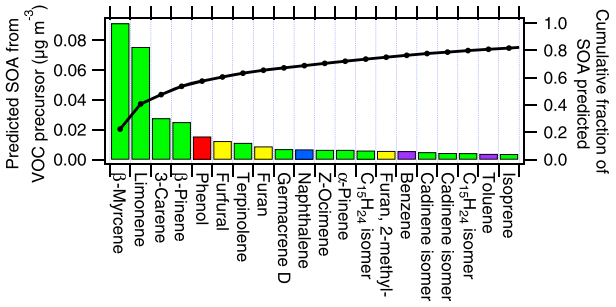

Figure 12. The cumulative SOA formed by each VOC for the aging of ponderosa pine smoke. The left axis is the cumulative SOA formed and the right shows the fraction of total SOA predicted. The coloring scheme is the same as in Figure 11.

Figure 11 also shows that incomplete combustion products, classified as substituted aromatics and polyaromatic hydrocarbons, are the next largest contributor to the SOA after biogenic compounds. However, their contribution is small relative to the monoterpenes for these foliar fuels. Not shown on this plot are the other 350+ VOCs that were quantified by GC × GC-TOFMS and modeled. Using the model, a minimum of 75

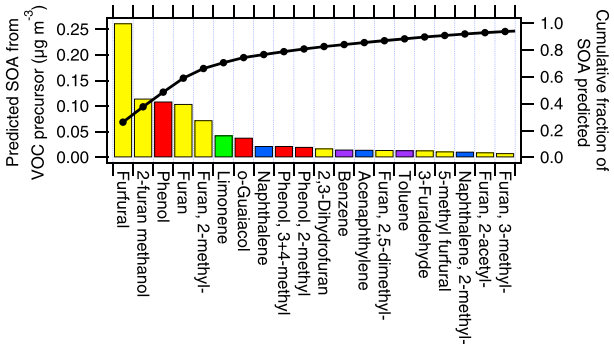

Figure 13. The cumulative SOA formed by each VOC for the aging of wiregrass smoke. The left axis is the cumulative SOA formed and the right shows the fraction of total SOA predicted. The coloring scheme is the same as in Figure 11.

VOCs are needed to explain 90% of the SOA mass formed. Figure 12 shows a similar distribution of SOA precursors for ponderosa pine smoke. More than 50% of the SOA formed was due to monoterpenes. Although other work has suggested that ponderosa pine fires emit more VOCs and therefore are likely to generate more SOA than black spruce, we observed large experiment-to-experiment variability (Hennigan et al., 2011). In experiments using black spruce smoke and UV lights ($n = 5$), the average OA enhancement and one standard deviation was 1.17 ± 0.17. The highest measured OA enhancement of these five black spruce smoke, UV-lights experiments was 1.49 and the lowest was 1.04; see Table 1. This degree of variability is consistent with the observations of Stockwell et al. (2014) that emission factors for VOCs for the same nominal fuel could vary ~40% from burn to burn during FLAME-IV.

3.5.2.2. Wiregrass

We observed very little SOA production from the aging of smoke from wiregrass. In Figure 13 we show the VOC-specific and cumulative SOA formed from the modeled aging of wiregrass smoke, using the same convention as Figure 11 described above. We predict just 1 $\mu g/m^3$ of SOA compared to 15 $\mu g/m^3$ from black spruce smoke. This is likely due to a combination of smaller emission rates and variable amounts of total smoke injected. Monoterpenes are much less abundant in wiregrass smoke and so contribute much less to SOA production compared to the coniferous canopy smoke. Consequently, oxygenated aromatics are relatively more important. The oxygenated aromatics may be the product of cellulose or lignin combustion (Collard & Blin, 2014). Cellulose is a naturally occurring polymer and its structure includes linked glucose monomers ($C_6H_{10}O_5$) (Pettersen, 1984). Combustion of glucose has been shown to form furans, for example, Figure 13, as well as oxygenated aromatics (Paine et al., 2008).

3.6. Trends in Oxidized VOCs With Aging

In addition to the oxidation of SOA precursors, we also measured the production of small oxidized VOCs that do not form SOA. Acetone was measured in real time by the PTR-MS at m/z 59 [M + H^+]. GC × GC-TOFMS also measured two additional isomers, which would also be detected by the PTR-MS at m/z 59, propanal and 2-propen-1-ol. Acetone is much more abundant in the fresh smoke; the other two isomers combined comprised were on average 1/6th the mass of acetone. In Figure 14, we report here the change in ion signal at m/z 59 using the calibration for acetone and risk overreporting changes in acetone concentration by not accounting for the potential the isomers. We believe this to be a good assumption because (a) acetone is a more favorable product of oxidation (more stable) and (b) it is more abundant in the measurements of fresh biomass burning.

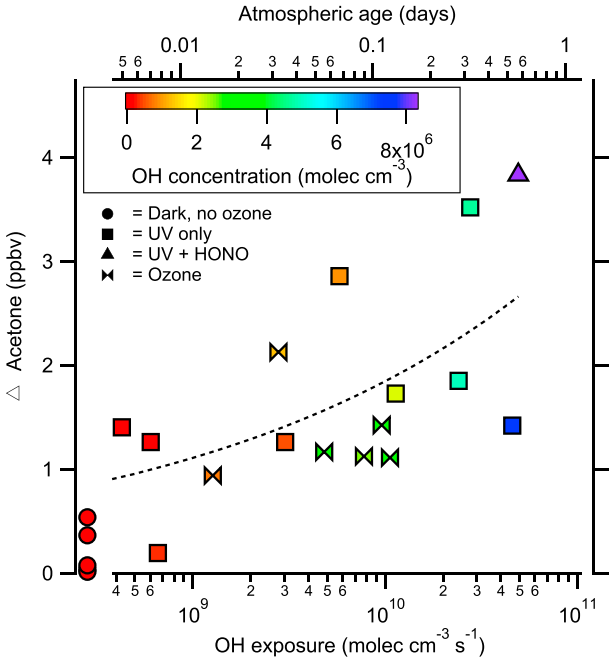

Figure 14. The difference in acetone concentrations measured by the PTR-MS before and after aging correlates well with OH exposure. OH concentration was calculated using the decay of toluene and a pseudo-first-order reaction rate law. An offset exponential function was fit to guide the eye: the change in acetone concentration as a result of aging (ppbv) = 0.126 + 0.00637 *[OH exposure]$^{0.243}$.

Figure 14 shows the increase in acetone that resulted from the aging of biomass burning aerosol as a function of OH exposure. The markers are colored by the calculated OH concentration and the marker shapes indicate the type of perturbation in the smog chamber. There is a positive correlation between OH exposure and the increase in acetone measured by the PTR-MS. A least squares fit of the increase in the acetone versus the natural log of the OH exposure has an $R^2 = 0.34$. This suggests that regardless of fuel, there is a consistent production of acetone when biomass burning smoke is aged by OH radicals, consistent with past ambient observations of aged smoke plumes (Holzinger et al., 2005; Karl et al., 2007). This correlation in acetone enhancement is notable in part due to the lack of correlation we observed comparing OH exposure to other oxidized VOCs measured by the PTR-MS, including methanol, formaldehyde, or acetaldehyde. Oxidized VOCs have previously been proposed as

an indicator for SOA formation; however, this work shows a strong correlation with OH exposure, rather than SOA formation (Lee et al., 2006). Our observations are consistent with work that shows the production of acetone during photodegradation of SOA (Lee et al., 2006; Malecha & Nizkorodov, 2016). However, our dark ozonolysis experiments also generated some acetone, consistent with SOA formation also yielding acetone as a by-product (Pan et al., 2009).

4. Conclusions

Measurements of OA mass enhancement in ambient biomass burning plumes are highly variable. We investigated SOA formation and multiphase POA oxidation in smoke from the open burning of various whole biomass fuels representative of canopy and grassland fires, using aging experiments in a dual smog-chamber system. We only observed significant OA enhancement from fuels representing canopy fires. These fresh fuels were dominated by foliage (needles) containing significant amounts of volatile precursors such as monoterpenes, in contrast to some other studies in the literature that focused on dried fuels in relatively controlled combustors (Bruns et al., 2016; Czech et al., 2017). We have found that in the controlled environment of a smog chamber, the OA enhancement following aging of the smoke can be predicted to within about a factor of 2 using a comprehensive fuel-specific VOC emission inventory that is scaled to the toluene concentration in a specific burn. We did not observe significant mass loss associated with POA volatilization in these experiments during the aging stage subsequent to the dilution caused by injection into the chamber.

We also found that for simulated coniferous-canopy smoke (which, in our experiments, was mainly from the combustion of fresh needles), biogenic VOCs (e.g., monoterpenes) were significant precursors for SOA production. This is in contrast to the findings of Bruns et al. (2016) and Tiitta et al. (2016), who could predict the SOA formation from fuel-wood-burning emissions using mostly pyrogenic VOCs (e.g., benzene, naphthalene, and toluene). These differences underscore the highly variable nature of SOA formation in biomass smoke: for fresh needle burning, biogenic VOCs appear to be dominant class of precursors; for the wiregrass fires, furans were the most important precursors; and, for fuel-wood fires, aromatics were the most important (Bruns et al., 2016). The relative importance of precursors will also likely vary by fuel moisture and combustion conditions. Because the fresh folial fuels were rich in VOCs, we found agreement between the predicted and measured OA enhancements to within a factor of 2; if anything, the model tended to predict slightly more SOA than we observed. The VOCs measured were sufficient to account for the variability in observed SOA mass in many experiments, despite evidence of a negative bias toward oxygenated VOCs in the Hatch et al. (2015) inventory (Hatch et al., 2017). We do not rule out a contribution to the SOA from IVOC oxidation, but the contributions from more volatile organic species are dominant in these experiments. Our results agree with those of Hatch et al. (2015) and show that open-burning biomass emissions require a more careful investigation of biogenic VOCs innate to the fuel. Given that most of the OA enhancement in these experiments can be explained by oxidation of VOC SOA precursors, we propose that future work should focus on determining VOC emission profiles and their consistency from the same fuel type (Hatch et al., 2017). Developing parameterizations for VOC emission profiles from the open burning of biomass fuels under different combustion conditions will improve predictions of the production of OA during atmospheric evolution of smoke plumes.

Acknowledgments
This research was supported in part by the DOE ASR (ER65296) and NSF (AGS-1256042), with instrumentation provided by NSF MRI (CBET-0922643) and the Wallace Research Foundation. The FLAME-IV experiment was supported by NSF (AGS-0936321). The authors thank the Fire Science Laboratory Staff and other FLAME-IV team members. In accordance with AGU data policy, processed data can be found in Table , the Supporting Information, and in companion papers Tkacik et al. (2017) and Hatch et al. (2015).

References

Ahern, A. T., Goldberger, L., Jahl, L., Thornton, J., & Sullivan, R. C. (2018). Production of N_2O_5 and $ClNO_2$ through nocturnal processing of biomass-burning aerosol. *Environmental Science & Technology*, *52*(2), 550–559. https://doi.org/10.1021/acs.est.7b04386

Aiken, A. C., de Foy, B., Wiedinmyer, C., DeCarlo, P. F., Ulbrich, I. M., Wehrli, M. N., et al. (2010). Mexico city aerosol analysis during MILAGRO using high resolution aerosol mass spectrometry at the urban supersite (T0)—Part 2: Analysis of the biomass burning contribution and the non-fossil carbon fraction. *Atmospheric Chemistry and Physics*, *10*(12), 5315–5341. https://doi.org/10.5194/acp-10-5315-2010

Aiken, A. C., Salcedo, D., Cubison, M. J., Huffman, J. A., DeCarlo, P. F., Ulbrich, I. M., et al. (2009). Mexico City aerosol analysis during MILAGRO using high resolution aerosol mass spectrometry at the urban supersite (T0)—Part 1: Fine particle composition and organic source apportionment. *Atmospheric Chemistry and Physics*, *9*(17), 6633–6653. https://doi.org/10.5194/acp-9-6633-2009

Akagi, S. K., Craven, J. S., Taylor, J. W., McMeeking, G. R., Yokelson, R. J., Burling, I. R., et al. (2012). Evolution of trace gases and particles emitted by a chaparral fire in California. *Atmospheric Chemistry and Physics*, *12*(3), 1397–1421. https://doi.org/10.5194/acp-12-1397-2012

Akagi, S. K., Yokelson, R. J., Wiedinmyer, C., Alvarado, M. J., Reid, J. S., Karl, T., et al. (2011). Emission factors for open and domestic biomass burning for use in atmospheric models. *Atmospheric Chemistry and Physics*, *11*(9), 4039–4072. https://doi.org/10.5194/acp-11-4039-2011

Andreae, M. O., & Merlet, P. (2001). Emission of trace gases and aerosols from biomass burning. *Global Biogeochemical Cycles*, *15*(4), 955–966. https://doi.org/10.1029/2000GB001382

Andreae, M. O., Rosenfeld, D., Artaxo, P., Costa, A. A., Frank, G. P., Longo, K. M., & Silva-Dias, M. A. F. (2004). Smoking rain clouds over the Amazon. *Science (New York, N.Y.)*, *303*(5662), 1337–1342. https://doi.org/10.1126/science.1092779

Atkinson, R., & Arey, J. (2003). Atmospheric degradation of volatile organic compounds. *Chemical Reviews*, *103*(12), 4605–4638. https://doi.org/10.1021/cr0206420

Bian, Q., May, A. A., Kreidenweis, S. M., & Pierce, J. R. (2015). Investigation of particle and vapor wall-loss effects on controlled wood-smoke smog-chamber experiments. *Atmospheric Chemistry and Physics*, *15*(19), 11,027–11,045. https://doi.org/10.5194/acp-15-11027-2015

Bond, T. C., Doherty, S. J., Fahey, D. W., Forster, P. M., Berntsen, T., DeAngelo, B. J., et al. (2013). Bounding the role of black carbon in the climate system: A scientific assessment. *Journal of Geophysical Research: Atmospheres*, *118*, 5380–5552. https://doi.org/10.1002/jgrd.50171

Bruns, E. A., El Haddad, I., Slowik, J. G., Kilic, D., Klein, F., Baltensperger, U., & Prévôt, A. S. H. (2016). Identification of significant precursor gases of secondary organic aerosols from residential wood combustion. *Scientific Reports*, *6*(1), 27881. https://doi.org/10.1038/srep27881

Canagaratna, M. R., Jimenez, J. L., Kroll, J. H., Chen, Q., Kessler, S. H., Massoli, P., et al. (2015). Elemental ratio measurements of organic compounds using aerosol mass spectrometry: Characterization, improved calibration, and implications. *Atmospheric Chemistry and Physics*, *15*(1), 253–272. https://doi.org/10.5194/acp-15-253-2015

Capes, G., Johnson, B., McFiggans, G., Williams, P. I., Haywood, J., & Coe, H. (2008). Aging of biomass burning aerosols over West Africa: Aircraft measurements of chemical composition, microphysical properties, and emission ratios. *Journal of Geophysical Research*, *113*, D00C15. https://doi.org/10.1029/2008JD009845

Chhabra, P. S., Flagan, R. C., & Seinfeld, J. H. (2010). Elemental analysis of chamber organic aerosol using an aerodyne high-resolution aerosol mass spectrometer. *Atmospheric Chemistry and Physics*, *10*(9), 4111–4131. https://doi.org/10.5194/acp-10-4111-2010

Collard, F.-X., & Blin, J. (2014). A review on pyrolysis of biomass constituents: Mechanisms and composition of the products obtained from the conversion of cellulose, hemicelluloses and lignin. *Renewable and Sustainable Energy Reviews*, *38*, 594–608. https://doi.org/10.1016/J.RSER.2014.06.013

Cubison, M. J., Ortega, A. M., Hayes, P. L., Farmer, D. K., Day, D., Lechner, M. J., et al. (2011). Effects of aging on organic aerosol from open biomass burning smoke in aircraft and laboratory studies. *Atmospheric Chemistry and Physics*, *11*(23), 12,049–12,064. https://doi.org/10.5194/acp-11-12049-2011

Czech, H., Pieber, S. M., Tiitta, P., Sippula, O., Kortelainen, M., Lamberg, H., et al. (2017). Time-resolved analysis of primary volatile emissions and secondary aerosol formation potential from a small-scale pellet boiler. *Atmospheric Environment*, *158*, 236–245. https://doi.org/10.1016/J.ATMOSENV.2017.03.040

Decarlo, P. F., Kimmel, J. R., Trimborn, A., Northway, M. J., Jayne, J. T., Aiken, A. C., et al. (2006). Field-depoloyable, high-resolution, time-of-flight aerosol mass spectrometer. *Analytical Chemistry*, *78*(24), 8281–8289. https://doi.org/8410.1029/2001JD001213.Analytical

DeCarlo, P. F., Slowik, J. G., Worsnop, D. R., Davidovits, P., & Jimenez, J. L. (2004). Particle morphology and density characterization by combined mobility and aerodynamic diameter measurements. Part 1: Theory. *Aerosol Science and Technology*, *38*(12), 1185–1205. https://doi.org/10.1080/027868290903907

DeCarlo, P. F., Ulbrich, I. M., Crounse, J., de Foy, B., Dunlea, E. J., Aiken, A. C., et al. (2010). Investigation of the sources and processing of organic aerosol over the Central Mexican Plateau from aircraft measurements during MILAGRO. *Atmospheric Chemistry and Physics*, *10*(12), 5257–5280. https://doi.org/10.5194/acp-10-5257-2010

Docherty, K. S., Aiken, A. C., Huffman, J. A., Ulbrich, I. M., DeCarlo, P. F., Sueper, D., et al. (2011). The 2005 Study of Organic Aerosols at Riverside (SOAR-1): Instrumental intercomparisons and fine particle composition. *Atmospheric Chemistry and Physics*, *11*(23), 12,387–12,420. https://doi.org/10.5194/acp-11-12387-2011

Docherty, K. S., Jaoui, M., Corse, E., Jimenez, J. L., Offenberg, J. H., Lewandowski, M., & Kleindienst, T. E. (2013). Collection efficiency of the aerosol mass spectrometer for chamber-generated secondary organic aerosols. *Aerosol Science and Technology*, *47*, 294–309. https://doi.org/10.1080/02786826.2012.752572

Donahue, N. M., Chuang, W., Epstein, S. A., Kroll, J. H., Worsnop, D. R., Robinson, A. L., et al. (2013). Why do organic aerosols exist? Understanding aerosol lifetimes using the two-dimensional volatility basis set. *Environmental Chemistry*, *10*(3), 151. https://doi.org/10.1071/EN13022

Donahue, N. M., Epstein, S. A., Pandis, S. N., & Robinson, A. L. (2011). A two-dimensional volatility basis set: 1. Organic-aerosol mixing thermodynamics. *Atmospheric Chemistry and Physics*, *11*(7), 3303–3318. https://doi.org/10.5194/acp-11-3303-2011

Donahue, N. M., Robinson, A. L., & Pandis, S. N. (2009). Atmospheric organic particulate matter: From smoke to secondary organic aerosol. *Atmospheric Environment*, *43*(1), 94–106. https://doi.org/10.1016/j.atmosenv.2008.09.055

Donahue, N. M., Robinson, A. L., Stanier, C. O., & Pandis, S. N. (2006). Coupled partitioning, dilution, and chemical aging of semivolatile organics. *Environmental Science & Technology*, *40*(8), 2635–2643. https://doi.org/10.1021/es052297c

Donahue, N. M., Robinson, A. L., Trump, E. R., Riipinen, I., & Kroll, J. H. (2012). *Volatility and aging of atmospheric organic aerosol*, (pp. 97–143). Berlin Heidelberg: Springer. https://doi.org/10.1007/128_2012_355

Donahue, N. M., Trump, E. R., Pierce, J. R., & Riipinen, I. (2011). Theoretical constraints on pure vapor-pressure driven condensation of organics to ultrafine particles. *Geophysical Research Letters*, *38*, L16801. https://doi.org/10.1029/2011GL048115

Farmer, D. K., Matsunaga, A., Docherty, K. S., Surratt, J. D., Seinfeld, J. H., Ziemann, P. J., & Jimenez, J. L. (2010). Response of an aerosol mass spectrometer to organonitrates and organosulfates and implications for atmospheric chemistry. *Proceedings of the National Academy of Sciences*, *107*(15), 6670–6675. https://doi.org/10.1073/pnas.0912340107

Fortenberry, C. F., Walker, M. J., Zhang, Y., Mitroo, D., Brune, W. H., & Williams, B. J. (2018). Bulk and molecular-level characterization of laboratory-aged biomass burning organic aerosol from oak leaf and heartwood fuels. *Atmospheric Chemistry and Physics*, *18*(3), 2199–2224. https://doi.org/10.5194/acp-18-2199-2018

Grieshop, A. P., Donahue, N. M., & Robinson, A. L. (2009). Laboratory investigation of photochemical oxidation of organic aerosol from wood fires. 2: Analysis of aerosol mass spectrometer data. *Atmospheric Chemistry and Physics*, *9*(6), 2227–2240. https://doi.org/10.5194/acp-9-2227-2009

Grieshop, A. P., Logue, J. M., Donahue, N. M., & Robinson, A. L. (2009). Laboratory investigation of photochemical oxidation of organic aerosol from wood fires. 1: Measurement and simulation of organic aerosol evolution. *Atmospheric Chemistry and Physics*, *9*(4), 1263–1277. https://doi.org/10.5194/acp-9-1263-2009

Hallquist, M., Wenger, J. C., Baltensperger, U., Rudich, Y., Simpson, D., Claeys, M., et al. (2009). The formation, properties and impact of secondary organic aerosol: Current and emerging issues. *Atmospheric Chemistry and Physics*, *9*(14), 5155–5236. https://doi.org/10.5194/acp-9-5155-2009

Hatch, L. E., Luo, W., Pankow, J. F., Yokelson, R. J., Stockwell, C. E., & Barsanti, K. C. (2015). Identification and quantification of gaseous organic compounds emitted from biomass burning using two-dimensional gas chromatography–time-of-flight mass spectrometry. *Atmospheric Chemistry and Physics*, *15*(4), 1865–1899. https://doi.org/10.5194/acp-15-1865-2015

Hatch, L. E., Yokelson, R. J., Stockwell, C. E., Veres, P. R., Simpson, I. J., Blake, D. R., et al. (2017). Multi-instrument comparison and compilation of non-methane organic gas emissions from biomass burning and implications for smoke-derived secondary organic aerosol precursors. *Atmospheric Chemistry and Physics*, *17*(2), 1471–1489. https://doi.org/10.5194/acp-17-1471-2017

Hatfield, M. L., & Huff Hartz, K. E. (2011). Secondary organic aerosol from biogenic volatile organic compound mixtures. *Atmospheric Environment*, *45*(13), 2211–2219. https://doi.org/10.1016/j.atmosenv.2011.01.065

Hays, M. D., Geron, C. D., Linna, K. J., Smith, N. D., & Schauer, J. J. (2002). Speciation of gas-phase and fine particle emissions from burning of foliar fuels. *Environmental Science & Technology*, *36*(11), 2281–2295. https://doi.org/10.1021/es0111683

Hennigan, C. J., Miracolo, M. A., Engelhart, G. J., May, A. A., Presto, A. A., Lee, T., et al. (2011). Chemical and physical transformations of organic aerosol from the photo-oxidation of open biomass burning emissions in an environmental chamber. *Atmospheric Chemistry and Physics*, *11*(15), 7669–7686. https://doi.org/10.5194/acp-11-7669-2011

Hennigan, C. J., Sullivan, A. P., Collett, J. L., & Robinson, A. L. (2010). Levoglucosan stability in biomass burning particles exposed to hydroxyl radicals. *Geophysical Research Letters*, *37*, L09806. https://doi.org/10.1029/2010GL043088

Heringa, M. F., DeCarlo, P. F., Chirico, R., Tritscher, T., Dommen, J., Weingartner, E., et al. (2011). Investigations of primary and secondary particulate matter of different wood combustion appliances with a high-resolution time-of-flight aerosol mass spectrometer. *Atmospheric Chemistry and Physics*, *11*(12), 5945–5957. https://doi.org/10.5194/acp-11-5945-2011

Hildebrandt, L., Donahue, N. M., & Pandis, S. N. (2009). High formation of secondary organic aerosol from the photo-oxidation of toluene. *Atmospheric Chemistry and Physics*, *9*(9), 2973–2986. https://doi.org/10.5194/acp-9-2973-2009

Holzinger, R., Williams, J., Salisbury, G., Klüpfel, T., de Reus, M., Traub, M., et al. (2005). Oxygenated compounds in aged biomass burning plumes over the Eastern Mediterranean: Evidence for strong secondary production of methanol and acetone. *Atmospheric Chemistry and Physics*, *5*(1), 39–46. https://doi.org/10.5194/acp-5-39-2005

Huffman, J. A., Ziemann, P. J., Jayne, J. T., Worsnop, D. R., Jimenez, J. L., Aiken, A., & Salcedo, D. (2008). Development and characterization of a fast-stepping/scanning thermodenuder for chemically-resolved aerosol volatility measurements. *Aerosol Science and Technology*, *42*(5), 395–407. https://doi.org/10.1080/02786820802104981

Jayne, J. T., Leard, D. C., Zhang, X., Davidovits, P., Smith, K. A., Kolb, C. E., & Worsnop, D. R. (2000). Development of an aerosol mass spectrometer for size and composition analysis of submicron particles. *Aerosol Science and Technology*, *33*(1–2), 49–70. https://doi.org/10.1080/027868200410840

Jimenez, J. L., Canagaratna, M. R., Donahue, N. M., Prevot, A. S. H., Zhang, Q., Kroll, J. H., et al. (2009). Evolution of organic aerosols in the atmosphere. *Science*, *326*(5959), 1525–1529. https://doi.org/10.1126/science.1180353

Jolleys, M. D., Coe, H., McFiggans, G., Capes, G., Allan, J. D., Crosier, J., et al. (2012). Characterizing the aging of biomass burning organic aerosol by use of mixing ratios: A meta-analysis of four regions. *Environmental Science & Technology.*, *46*(24), 13,093–13,102. https://doi.org/10.1021/es302386v

Kari, E., Hao, L., Yli-Pirilä, P., Leskinen, A., Kortelainen, M., Grigonyte, J., et al. (2017). Effect of pellet boiler exhaust on secondary organic aerosol formation from α-pinene. *Environmental Science & Technology*, *51*(3), 1423–1432. https://doi.org/10.1021/acs.est.6b04919

Karl, T. G., Christian, T. J., Yokelson, R. J., Artaxo, P., Hao, W. M., & Guenther, A. (2007). The Tropical Forest and Fire Emissions Experiment: Method evaluation of volatile organic compound emissions measured by PTR-MS, FTIR, and GC from tropical biomass burning. *Atmospheric Chemistry and Physics*, *7*(22), 5883–5897. https://doi.org/10.5194/acp-7-5883-2007

Kortelainen, M., Jokiniemi, J., Tiitta, P., Tissari, J., Lamberg, H., Leskinen, J., et al. (2018). Time-resolved chemical composition of small-scale batch combustion emissions from various wood species. *Fuel*, *233*, 224–236. https://doi.org/10.1016/J.FUEL.2018.06.056

Krechmer, J. E., Pagonis, D., Ziemann, P. J., & Jimenez, J. L. (2016). Quantification of gas-wall partitioning in Teflon environmental chambers using rapid bursts of low-volatility oxidized species generated in situ. *Environmental Science & Technology*, *50*(11), 5757–5765. https://doi.org/10.1021/acs.est.6b00606

Lee, A., Goldstein, A. H., Kroll, J. H., Ng, N. L., Varutbangkul, V., Flagan, R. C., & Seinfeld, J. H. (2006). Gas-phase products and secondary aerosol yields from the photooxidation of 16 different terpenes. *Journal of Geophysical Research*, *111*, D17305. https://doi.org/10.1029/2006JD007050

Lee, T., Sullivan, A. P., Mack, L., Jimenez, J. L., Kreidenweis, S. M., Onasch, T. B., et al. (2010). Chemical smoke marker emissions during flaming and smoldering phases of laboratory open burning of wildland fuels. *Aerosol Science and Technology*, *44*(9), i–v. https://doi.org/10.1080/02786826.2010.499884

Malecha, K. T., & Nizkorodov, S. A. (2016). Photodegradation of secondary organic aerosol particles as a source of small, oxygenated volatile organic compounds. *Environmental Science & Technology*, *50*(18), 9990–9997. https://doi.org/10.1021/acs.est.6b02313

Matsunaga, A., & Ziemann, P. J. (2010). Gas-wall partitioning of organic compounds in a Teflon film chamber and potential effects on reaction product and aerosol yield measurements. *Aerosol Science and Technology*, *44*(10), 881–892. https://doi.org/10.1080/02786826.2010.501044

May, A. A., Levin, E. J. T., Hennigan, C. J., Riipinen, I., Lee, T., Collett, J. L., et al. (2013). Gas-particle partitioning of primary organic aerosol emissions: 3. Biomass burning. *Journal of Geophysical Research: Atmospheres*, *118*, 11,327–11,338. https://doi.org/10.1002/jgrd.50828

May, A. A., Saleh, R., Hennigan, C. J., Donahue, N. M., & Robinson, A. L. (2012). Volatility of organic molecular markers used for source apportionment analysis: Measurements and implications for atmospheric lifetime. *Environmental Science and Technology*, *46*(22), 12,435–12,444. https://doi.org/10.1021/es302276t

McMeeking, G. R., Kreidenweis, S. M., Baker, S., Carrico, C. M., Chow, J. C., Collett, J. L., et al. (2009). Emissions of trace gases and aerosols during the open combustion of biomass in the laboratory. *Journal of Geophysical Research*, *114*, D19210. https://doi.org/10.1029/2009JD011836

McMurry, P. H., & Grosjean, D. (1985). Gas and aerosol wall losses in Teflon film smog chambers. *Environmental Science & Technology*, *19*(12), 1176–1182. https://doi.org/10.1021/es00142a006

Mohr, C., DeCarlo, P. F., Heringa, M. F., Chirico, R., Slowik, J. G., Richter, R., et al. (2012). Identification and quantification of organic aerosol from cooking and other sources in Barcelona using aerosol mass spectrometer data. *Atmospheric Chemistry and Physics*, *12*(4), 1649–1665. https://doi.org/10.5194/acp-12-1649-2012

Ng, N. L., Canagaratna, M. R., Zhang, Q., Jimenez, J. L., Tian, J., Ulbrich, I. M., et al. (2010). Organic aerosol components observed in Northern Hemispheric datasets from Aerosol Mass Spectrometry. *Atmospheric Chemistry and Physics*, *10*(10), 4625–4641. https://doi.org/10.5194/acp-10-4625-2010

Ng, N. L., Chhabra, P. S., Chan, A. W. H., Surratt, J. D., Kroll, J. H., Kwan, A. J., et al. (2007). Effect of NO_x level on secondary organic aerosol (SOA) formation from the photooxidation of terpenes. *Atmospheric Chemistry and Physics*, *7*(19), 5159–5174. https://doi.org/10.5194/acp-7-5159-2007

Odum, J., Hoffman, T., Bowman, F., Collins, D., Flagan, R., & Seinfeld, J. H. (1996). Gas/particle partitioning and secondary organic aerosol yields. *Environmental Science and Technology*, *30*(8), 2580–2585. https://doi.org/doi:10.1021/ES950943+

Ortega, A. M., Day, D. A., Cubison, M. J., Brune, W. H., Bon, D., de Gouw, J. A., & Jimenez, J. L. (2013). Secondary organic aerosol formation and primary organic aerosol oxidation from biomass-burning smoke in a flow reactor during FLAME-3. *Atmospheric Chemistry and Physics*, *13*(22), 11,551–11,571. https://doi.org/10.5194/acp-13-11551-2013

Paine, J. B., Pithawalla, Y. B., & Naworal, J. D. (2008). Carbohydrate pyrolysis mechanisms from isotopic labeling: Part 4. The pyrolysis of d-glucose—The formation of furans. *Journal of Analytical and Applied Pyrolysis*, *83*(1), 37–63. https://doi.org/10.1016/j.jaap.2008.05.008

Pan, X., Underwood, J. S., Xing, J. H., Mang, S. A., & Nizkorodov, S. A. (2009). Photodegradation of secondary organic aerosol generated from limonene oxidation by ozone studied with chemical ionization mass spectrometry. *Atmospheric Chemistry and Physics*, *9*(12), 3851–3865. https://doi.org/10.5194/acp-9-3851-2009

Pankow, J. F. (1994). An absorption model of the gas/aerosol partitioning involved in the formation of secondary organic aerosol. *Atmospheric Environment*, *28*(2), 189–193. https://doi.org/10.1016/1352-2310(94)90094-9

Pettersen, R. C. (1984). The chemical composition of wood (pp. 57–126). https://doi.org/10.1021/ba-1984-0207.ch002

Presto, A. A., & Donahue, N. M. (2006). Investigation of α-pinene + ozone secondary organic aerosol formation at low total aerosol mass. *Environmental Science & Technology*, *40*(11), 3536–3543. https://doi.org/10.1021/es052203z

Presto, A. A., Huff Hartz, K. E., & Donahue, N. M. (2005). Secondary organic aerosol production from terpene ozonolysis. 2. Effect of NO_x concentration. *Environmental Science & Technology*, *39*(18), 7046–7054. https://doi.org/10.1021/es050400s

Presto, A. A., Miracolo, M. A., Kroll, J. H., Worsnop, D. R., Robinson, A. L., & Donahue, N. M. (2009). Intermediate-volatility organic compounds: A potential source of ambient oxidized organic aerosol. *Environmental Science & Technology*, *43*(13), 4744–4749. https://doi.org/10.1021/es803219q

Radke, L. F., Hegg, D. A., Hobbs, P. V., Nance, J. D., Lyons, J. H., Laursen, K. K., et al. (1991). Particulate and trace gas emissions from large biomass fires in North America. *Global Biomass Burning: Atmospheric, Climatic, and Biospheric Implications*, *5*, 219–220. Retrieved fromhttps://www.researchgate.net/profile/Philip_Riggan/publication/247117229_Particulate_and_trace_gas_emissions_from_large_biomass_fires_in_North_America/links/53e929050cf28f342f3f7c82/Particulate-and-trace-gas-emissions-from-large-biomass-fires-in-North-Ame

Reid, J. S., Hobbs, P. V., Ferek, R. J., Blake, D. R., Martins, J. V., Dunlap, M. R., & Liousse, C. (1998). Physical, chemical, and optical properties of regional hazes dominated by smoke in Brazil. *Journal of Geophysical Research*, *103*(D24), 32,059–32,080. https://doi.org/10.1029/98JD00458

Reid, J. S., Koppmann, R., Eck, T. F., & Eleuterio, D. P. (2005). A review of biomass burning emissions. Part II: Intensive physical properties of biomass burning particles. *Atmospheric Chemistry and Physics*, *5*(3), 799–825. https://doi.org/10.5194/acp-5-799-2005

Robinson, A. L., Donahue, N. M., Shrivastava, M. K., Weitkamp, E. A., Sage, A. M., Grieshop, A. P., et al. (2007). Rethinking organic aerosols: Semivolatile emissions and photochemical aging. *Science*, *315*(5816), 1259–1262. https://doi.org/10.1126/science.1133061

Robinson, E. S., Onasch, T. B., Worsnop, D., & Donahue, N. M. (2017). Collection efficiency of α-pinene secondary organic aerosol particles explored via light-scattering single-particle aerosol mass spectrometry. *Atmospheric Measurement Techniques*, *10*(3), 1139–1154. https://doi.org/10.5194/amt-10-1139-2017

Sage, A. M., Weitkamp, E. A., Robinson, A. L., & Donahue, N. M. (2008). Evolving mass spectra of the oxidized component of organic aerosol: Results from aerosol mass spectrometer analyses of aged diesel emissions. *8*(5), 1139–1152. https://doi.org/10.5194/acp-8-1139-2008

Saleh, R., Donahue, N. M., & Robinson, A. L. (2013). Time scales for gas-particle partitioning equilibration of secondary organic aerosol formed from alpha-pinene ozonolysis. *Environmental Science & Technology*, *47*(11), 5588–5594. https://doi.org/10.1021/es400078d

Saleh, R., Hennigan, C. J., Mcmeeking, G. R., Chuang, W. K., Robinson, E. S., Coe, H., et al. (2013). Absorptivity of brown carbon in fresh and photo-chemically aged biomass-burning emissions. *Atmospheric Chemistry and Physics*, *13*(15), 7683–7693. https://doi.org/10.5194/acp-13-7683-2013

Saleh, R., Robinson, E. S., Tkacik, D. S., Ahern, A. T., Liu, S., Aiken, A. C., et al. (2014). Brownness of organics in aerosols from biomass burning linked to their black carbon content. *Nature Geoscience*, *7*(9), 647–650. https://doi.org/10.1038/ngeo2220

Schauer, J. J., Kleeman, M. J., Cass, G. R., & Simoneit, B. R. T. (2001). Measurement of emissions from air pollution sources. 3; C1-C29 organic compounds from fireplace combustion of wood. *Environmental Science and Technology*, *35*(9), 1716–1728. https://doi.org/10.1021/es001331e

Schurman, M. I., Lee, T., Desyaterik, Y., Schichtel, B. A., Kreidenweis, S. M., & Collett, J. L. (2015). Transport, biomass burning, and in-situ formation contribute to fine particle concentrations at a remote site near Grand Teton National Park. *Atmospheric Environment*, *112*, 257–268. https://doi.org/10.1016/J.ATMOSENV.2015.04.043

Seinfeld, J. H., & Pandis, S. N. (1998). *Atmospheric chemistry and physics from air pollution to climate change*. Hoboken, NJ: John Wiley & Sons. https://doi.org/10.1016/0016-7037(87)90252-3

Simoneit, B. R. T., Schauer, J. J., Nolte, C. G., Oros, D. R., Elias, V. O., Fraser, M. P., et al. (1999). Levoglucosan, a tracer for cellulose in biomass burning and atmospheric particles. *Atmospheric Environment*, *33*(2), 173–182. https://doi.org/10.1016/S1352-2310(98)00145-9

Sinha, A., Saleh, R., Robinson, E. S., Ahern, A. T., Tkacik, D. S., Presto, A. A., et al. (2017). Mass accommodation coefficients of fresh and aged biomass-burning emissions. *Aerosol Science and Technology*, *52*(3), 300–309. https://doi.org/10.1080/02786826.2017.1413488

Stockwell, C. E., Christian, T. J., Goetz, J. D., Jayarathne, T., Bhave, P. V., Praveen, P. S., et al. (2016). Nepal Ambient Monitoring and Source Testing Experiment (NAMaSTE): Emissions of trace gases and light-absorbing carbon from wood and dung cooking fires, garbage and crop residue burning, brick kilns, and other sources. *Atmospheric Chemistry and Physics*, *16*(17), 11,043–11,081. https://doi.org/10.5194/acp-16-11043-2016

Stockwell, C. E., Veres, P. R., Williams, J., & Yokelson, R. J. (2015). Characterization of biomass burning emissions from cooking fires, peat, crop residue, and other fuels with high-resolution proton-transfer-reaction time-of-flight mass spectrometry. *Atmospheric Chemistry and Physics*, *15*(2), 845–865. https://doi.org/10.5194/acp-15-845-2015

Stockwell, C. E., Yokelson, R. J., Kreidenweis, S. M., Robinson, A. L., DeMott, P. J., Sullivan, R. C., et al. (2014). Trace gas emissions from combustion of peat, crop residue, domestic biofuels, grasses, and other fuels: Configuration and Fourier transform infrared (FTIR)

component of the fourth Fire Lab at Missoula Experiment (FLAME-4). *Atmospheric Chemistry and Physics*, *14*(18), 9727–9754. https://doi.org/10.5194/acp-14-9727-2014

Sullivan, A. P., Holden, A. S., Patterson, L. A., Mcmeeking, G. R., Kreidenweis, S. M., Malm, W. C., et al. (2008). A method for smoke marker measurements and its potential application for determining the contribution of biomass burning from wildfires and prescribed fires to ambient PM 2.5 organic carbon. *Journal of Geophysical Research*, *113*, D22302. https://doi.org/10.1029/2008JD010216

Tiitta, P., Leskinen, A., Hao, L., Yli-Pirilä, P., Kortelainen, M., Grigonyte, J., et al. (2016). Transformation of logwood combustion emissions in a smog chamber: Formation of secondary organic aerosol and changes in the primary organic aerosol upon daytime and nighttime aging. *Atmospheric Chemistry and Physics*, *16*(20), 13,251–13,269. https://doi.org/10.5194/acp-16-13251-2016

Tkacik, D. S., Robinson, E. S., Ahern, A., Saleh, R., Stockwell, C., Veres, P., et al. (2017). A dual-chamber method for quantifying the effects of atmospheric perturbations on secondary organic aerosol formation from biomass burning emissions. *Journal of Geophysical Research: Atmospheres*, *122*, 6043–6058. https://doi.org/10.1002/2016JD025784

Trump, E. R., Epstein, S. A., Riipinen, I., & Donahue, N. M. (2016). Wall effects in smog chamber experiments: A model study. *Aerosol Science and Technology*, *50*(11), 1180–1200. https://doi.org/10.1080/02786826.2016.1232858

Ulbrich, I. M., Canagaratna, M. R., Zhang, Q., Worsnop, D. R., & Jimenez, J. L. (2009). Interpretation of organic components from Positive Matrix Factorization of aerosol mass spectrometric data. *Atmospheric Chemistry and Physics*, *9*(9), 2891–2918. https://doi.org/10.5194/acp-9-2891-2009

Vakkari, V., Kerminen, V.-M., Beukes, J. P., Tiitta, P., van Zyl, P. G., Josipovic, M., et al. (2014). Rapid changes in biomass burning aerosols by atmospheric oxidation. *Geophysical Research Letters*, *41*, 2644–2651. https://doi.org/10.1002/2014GL059396

Weitkamp, E. A., Sage, A. M., Pierce, J. R., Donahue, N. M., & Robinson, A. L. (2007). Organic aerosol Formation from photochemical oxidation of diesel exhaust in a smog chamber. *Environmental Science & Technology*, *41*(20), 6969–6975. https://doi.org/10.1021/es070193r

Ye, P., Ding, X., Hakala, J., Hofbauer, V., Robinson, E. S., & Donahue, N. M. (2016). Vapor wall loss of semi-volatile organic compounds in a Teflon chamber. *Aerosol Science and Technology*, *50*(8), 822–834. https://doi.org/10.1080/02786826.2016.1195905

Yokelson, R. J., Bertschi, I. T., Christian, T. J., Hobbs, P. V., Ward, D. E., & Hao, W. M. (2003). Trace gas measurements in nascent, aged, and cloud-processed smoke from African savanna fires by airborne Fourier transform infrared spectroscopy (AFTIR). *Journal of Geophysical Research*, *108*(D13), 8478. https://doi.org/10.1029/2002JD002322

Yokelson, R. J., Crounse, J. D., DeCarlo, P. F., Karl, T., Urbanski, S., Atlas, E., et al. (2009). Emissions from biomass burning in the Yucatan. *Atmospheric Chemistry and Physics*, *9*(15), 5785–5812. https://doi.org/10.5194/acp-9-5785-2009

Zhang, X., Cappa, C. D., Jathar, S. H., McVay, R. C., Ensberg, J. J., Kleeman, M. J., & Seinfeld, J. H. (2014). Influence of vapor wall loss in laboratory chambers on yields of secondary organic aerosol. *Proceedings of the National Academy of Sciences of the United States of America*, *111*(16), 5802–5807. https://doi.org/10.1073/pnas.1404727111

Zhao, Y., Hennigan, C. J., May, A. A., Tkacik, D. S., de Gouw, J. A., Gilman, J. B., et al. (2014). Intermediate-volatility organic compounds: A large source of secondary organic aerosol. *Environmental Science & Technology*, *48*(23), 13,743–13,s750. https://doi.org/10.1021/es5035188